Imatinib inhibits VEGF-independent angiogenesis by targeting neuropilin 1–dependent ABL1 activation in endothelial cells

Claudio Raimondi,[1] Alessandro Fantin,[1] Anastasia Lampropoulou,[1] Laura Denti,[1] Anissa Chikh,[2] and Christiana Ruhrberg[1]

[1]UCL Institute of Ophthalmology, University College London, London EC1V 9EL, England UK
[2]Centre for Cutaneous Research, Blizard Institute, Barts and The London School of Medicine and Dentistry, Queen Mary London University, London E1 2AT, England UK

To enable new blood vessel growth, endothelial cells (ECs) express neuropilin 1 (NRP1), and NRP1 associates with the receptor tyrosine kinase VEGFR2 after binding the vascular endothelial growth factor A (VEGF) to enhance arteriogenesis. We report that NRP1 contributes to angiogenesis through a novel mechanism. In human and mouse ECs, the integrin ligand fibronectin (FN) stimulated actin remodeling and phosphorylation of the focal adhesion component paxillin (PXN) in a VEGF/VEGFR2-independent but NRP1-dependent manner. NRP1 formed a complex with ABL1 that was responsible for FN-dependent PXN activation and actin remodeling. This complex promoted EC motility in vitro and during angiogenesis on FN substrates in vivo. Accordingly, both physiological and pathological angiogenesis in the retina were inhibited by treatment with Imatinib, a small molecule inhibitor of ABL1 which is widely used to prevent the proliferation of tumor cells that express BCR-ABL fusion proteins. The finding that NRP1 regulates angiogenesis in a VEGF- and VEGFR2-independent fashion via ABL1 suggests that ABL1 inhibition provides a novel opportunity for anti-angiogenic therapy to complement VEGF or VEGFR2 blockade in eye disease or solid tumor growth.

CORRESPONDENCE
Claudio Raimondi:
c.raimondi@ucl.ac.uk
OR
Christiana Ruhrberg:
c.ruhrberg@ucl.ac.uk

Abbreviations used: AMD, age-related macular degeneration; AV, avascular area; EC, endothelial cell; ECM, extracellular matrix; FN, fibronectin; HDMEC, human dermal microvascular EC; HUVEC, human umbilical vein EC; MLEC, mouse lung EC; NRP1, neuropilin 1; OIR, oxygen-induced retinopathy; PDR, proliferative diabetic retinopathy; PXN, paxillin; ROP, retinopathy of prematurity; VEGF, vascular endothelial growth factor.

New blood vessels arise from preexisting ones in the process of physiological angiogenesis, both during embryonic development and in the female reproductive cycle. In addition, angiogenic vessel growth is closely associated with the progression of various cancers and eye diseases (Welti et al., 2013). Thus, angiogenesis promotes the growth of solid tumors and their metastasis, whereas abnormal blood vessel growth in the eye impairs visual function. For example, abnormal choroidal angiogenesis is a pathological feature of the "wet" form of age-related macular degeneration (AMD), whereas excessive retinal angiogenesis leads to vascular malformations that protrude into the vitreous in patients with proliferative diabetic retinopathy (PDR) or retinopathy of prematurity (ROP; Campochiaro, 2013).

The vascular endothelial growth factor A (VEGF) is a key mediator of both physiological and pathological angiogenesis and a validated target for anti-angiogenesis therapy in the clinic (Kim and D'Amore, 2012; Welti et al., 2013). For example, anti-VEGF therapy stabilized sight in >90% and significantly improved vision in ∼30% of patients with wet AMD over a 2-yr treatment period (Rosenfeld et al., 2006). However, the efficacy of anti-VEGF in AMD has been mainly attributed to reduced vascular leak rather than to an effect on neoangiogenesis (Campochiaro, 2013). The incomplete sensitivity of pathological eye vessels to anti-VEGF therapy may suggest that VEGF-independent pathways also contribute to ocular angiogenesis. Moreover, long-term anti-VEGF treatment has been proposed to pose likely risks, as preclinical studies for several different eye diseases revealed excessive neuronal cell death in the retina after VEGF blockade (Nishijima et al., 2007; Saint-Geniez et al., 2008; Foxton et al., 2013). Yet clinical data from long-term studies

C. Raimondi and A. Fantin contributed equally to this paper.

The Rockefeller University Press $30.00
J. Exp. Med. 2014 Vol. 211 No. 6 1167-1183
www.jem.org/cgi/doi/10.1084/jem.20132330

The Journal of Experimental Medicine

of patients with continuous anti-VEGF treatment are not available. These considerations, combined with the observation that tumor vessels can develop resistance to anti-VEGF therapy (Casanovas et al., 2005; Shojaei et al., 2007), highlight the need to identify effective anti-angiogenesis therapies that are based on VEGF-independent targets and can be used in combination with or independently of anti-VEGF therapy to improve outcome for patients.

Neuropilin 1 (NRP1) is a non-catalytic receptor for the VEGF165 isoform of VEGF that complexes with VEGFR2 to potentiate signal transduction in endothelial cells (ECs; e.g., Mamluk et al., 2002; Koch et al., 2011). Thus, the NRP1 cytoplasmic tail recruits a trafficking complex that directs VEGFR2 along an endocytic pathway that prevents receptor dephosphorylation to augment MAPK signaling via ERK1 and ERK2 (Salikhova et al., 2008; Ballmer-Hofer et al., 2011; Lanahan et al., 2013). This NRP1 function is essential for arteriogenesis, which depends on luminal vessel growth, but is dispensable for angiogenesis, driven by vessel sprouting, branching, and fusion (Fantin et al., 2011; Lanahan et al., 2013). Additionally, NRP1 is able to interact with extracellular matrix (ECM) receptors of the integrin family independently of VEGFR2 (Murga et al., 2005; Fukasawa et al., 2007; Valdembri et al., 2009). However, the relative significance of NRP1 for VEGF/VEGFR2-dependent versus integrin ligand-stimulated, but VEGFR2-independent processes for angiogenesis in vivo has not previously been determined. Moreover, the intracellular pathways that may be regulated by NRP1 in a VEGF/VEGFR2-independent fashion have, surprisingly, not yet been defined.

Here, we demonstrate that NRP1 promotes the phosphorylation of integrin targets such as paxillin (PXN) and concomitant actin remodeling in fibronectin (FN)-stimulated human ECs. Rather than using VEGFR2, NRP1-dependent PXN activation was found to rely on NRP1 association with ABL1, a nonreceptor tyrosine kinase with an actin-binding/bundling domain that links phosphoregulation to actin remodeling in a diverse range of cell types (Colicelli, 2010). Accordingly, knockdown of NRP1 or ABL1 by siRNA technology or with genetic tools inhibited actin remodeling and PXN phosphorylation, and consequently the migration of human and mouse ECs on FN in vitro. Inhibition of ABL1 kinase activity with Imatinib, an FDA-approved drug used to treat cell proliferation in leukemia caused by ABL1-BCR fusion protein, demonstrated similar effects on ECs in vitro and reduced vascular sprouting and branching on FN-rich templates during angiogenesis in vivo. Moreover, Imatinib treatment curbed pathological blood vessel growth in a mouse model of neovascular eye disease similarly to targeting NRP1 in ECs. ABL1 therefore presents a novel therapeutic opportunity for anti-angiogenic therapy.

RESULTS

NRP1 promotes spreading and actin remodeling of FN-stimulated ECs independently of roles in cell adhesion and VEGFR2

Because NRP1 is known to interact with FN-binding integrins (Fukasawa et al., 2007; Robinson et al., 2009; Valdembri et al., 2009), we first examined the requirement of NRP1 for EC adhesion, spreading, and actin remodeling. For these experiments, we used human dermal microvascular ECs (HDMECs) because dermal vasculature naturally undergoes extensive angiogenesis during wound healing. We additionally used human umbilical vein ECs (HUVECs), as they have been widely used to study VEGF-induced signaling mechanisms (e.g., Soker et al., 2002; Pan et al., 2007a; Chen et al., 2010). We transfected primary cells with a previously validated siRNA that targets NRP1 or a control nonsense siRNA. Having confirmed the efficacy of this approach (Fig. 1 A), we tested HDMEC and HUVEC adhesion to tissue culture dishes coated with 10 µg/ml FN, a concentration which effectively promotes cell adhesion and migration (Clark et al., 1986; Sottile et al., 1998; Tvorogov et al., 2005). In contrast to earlier studies, which reported that NRP1 loss inhibits HUVEC adhesion at FN concentrations <5 µg/ml (Murga et al., 2005; Valdembri et al., 2009), we found that adhesion was not compromised by NRP1 deficiency in either HDMECs or HUVECs at 10 µg/ml FN (Fig. 1, B and C). We had therefore identified conditions suitable to study FN-induced cell spreading, actin remodeling, and cell migration of ECs in the absence of prior defects in cell attachment.

Phalloidin staining of filamentous (F) actin showed that NRP1-deficient HDMECs (Fig. 1, D and E) adopted an abnormal round morphology with abundant cortical actin when plated on FN (Fig. 1 F). In contrast, control cells appeared elongated and contained stress fibers typical of adherent cells (Fig. 1 F). VEGFR2 protein levels (Fig. 1 D) and mRNA expression (Fig. 1 E) were slightly but significantly decreased in NRP1-deficient cells, but cells transfected with siRNA targeting VEGFR2 spread well on FN and assembled many stress fibers (Fig. 1 F), indicating that cytoskeletal defects in NRP1-deficient cells were not caused by low VEGFR2 expression. High magnification images revealed phalloidin-positive, filopodia-like microspikes in HDMECs 60 and 120 min after plating on FN, which were significantly reduced after NRP1 but not VEGFR2 down-regulation (Fig. 1 F, right columns). Quantitation confirmed that NRP1 but not VEGFR2 down-regulation significantly impaired cell spreading (Fig. 1 G) and microspike extension (Fig. 1 H) in cells plated on FN. Strikingly, addition of VEGF165, which is known to bind both VEGFR2 and NRP1, did not rescue the cytoskeletal defects of FN-stimulated HDMECs lacking NRP1 (Fig. 1 I). NRP1 therefore functions independently of VEGF and VEGFR2 to regulate ECM-induced cell spreading and actin remodeling in ECs.

NRP1 promotes the motility and haptotactic migration of FN-stimulated ECs

Impaired cell spreading and actin remodeling in NRP1-deficient ECs predicts defective cell motility. By tracking the behavior of individual HDMECs after plating on FN, we indeed found that control cells were significantly more motile than cells lacking NRP1 (Videos 1 and 2; Fig. 1, J and K). Consistent with reduced motility, transwell assay measuring ECM-induced

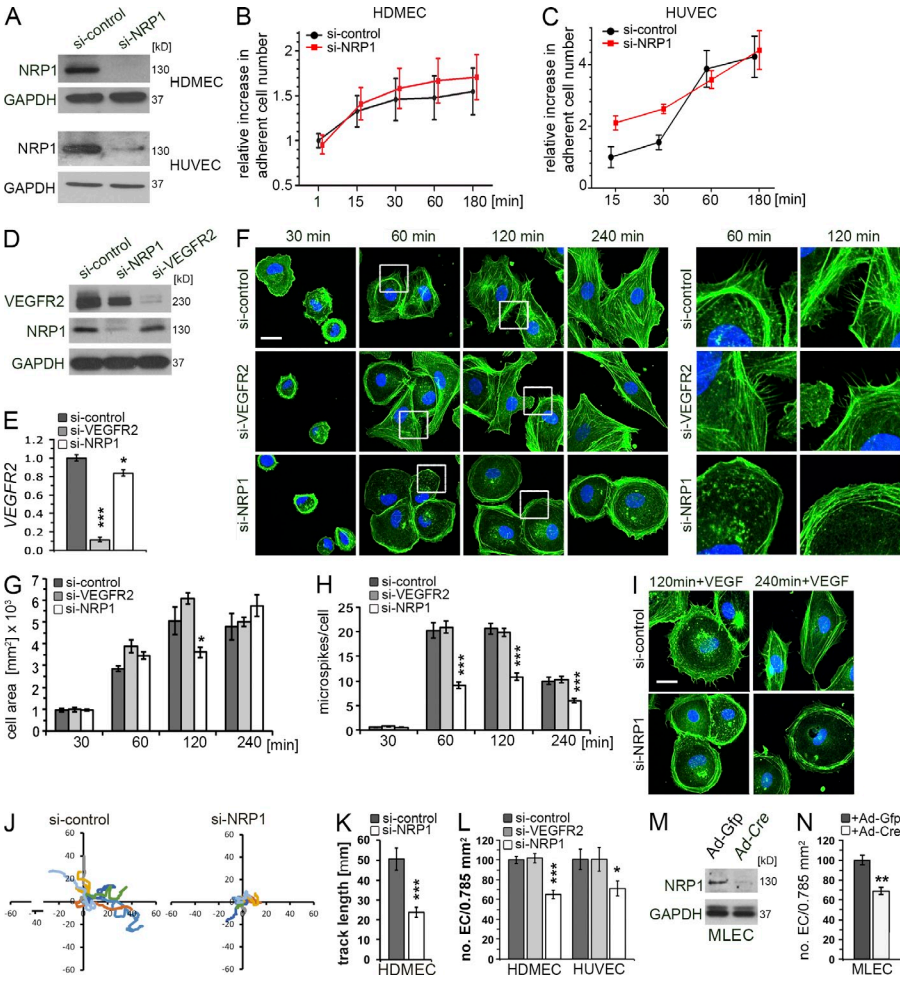

Figure 1. NRP1 is dispensable for cell matrix adhesion but promotes FN-induced cell spreading, filopodia extension, and motility of primary ECs. (A–C) Immunoblotting with the indicated antibodies to demonstrate NRP1 knockdown (A) and time course of cell adhesion (B and C) in HDMECs and HUVECs transfected with control or NRP1 siRNA and plated for the indicated times on plastic dishes coated with 10 µg/ml FN (mean ± SEM of 3 independent experiments). (D–H) HDMECs transfected with control, VEGFR2 or NRP1 siRNA were plated on FN for the indicated times before immunoblotting (D), qPCR analysis (E) or fluorescent labeling (F) with the F-actin marker phalloidin (green) and the nuclear counterstain DAPI (blue). Bar, 20 µm. Images shown in the right two columns are higher magnifications of areas indicated with dotted squares. Also shown is a quantification of cell area (G) and phalloidin-stained microspikes (H) at the indicated time points (mean ± SEM of ≥30 cells from 3 independent experiments). (I) HDMECs transfected with si-NRP1 were plated on FN in the presence of 50 ng/ml VEGF165 for the indicated times before fluorescent labeling with phalloidin (green) and DAPI (blue). Bar, 20 µm. (J and K) HDMECs transfected with control or NRP1 siRNAs were plated on FN and cell motility on FN observed for 200 min. J shows representative tracks, with the point of origin of each cell plotted as 0 at the axis intersection. K shows mean track length (mean ± SEM of 23 cells from 2 independent experiments). (L–N) HDMECs or HUVECs transfected with control, VEGFR2 or NRP1 siRNA (L) and *Nrp1*$^{fl/fl}$ MLECs transfected with adenovirus carrying *Gfp* control or *Cre* transgenes (M and N) were plated on FN-coated transwells. The number of transmigrated cells was determined after 240 min (mean ± SEM from ≥3 experiments, each performed in duplicate). Asterisks indicate statistical significance: *, P < 0.05; **, P < 0.01; ***, P < 0.001, Student's *t* test.

haptotaxis demonstrated reduced migration of NRP1-deficient compared with control cells toward FN, but VEGFR2 knockdown did not affect migration (Fig. 1 L). Similar results were obtained with HUVECs (Fig. 1 L). To examine if NRP1 deficiency impaired EC migration in another species, we used mouse lung ECs (MLECs) from *Nrp1* conditional null (*Nrp1*$^{fl/fl}$) mice in the transwell assay after infecting them with adenovirus expressing GFP as a control or CRE recombinase to down-regulate NRP1 (Fig. 1 M). As observed for human ECs, migration onto FN substrates was significantly reduced in MLECs lacking NRP1 compared with controls (Fig. 1 N). NRP1 deficiency therefore impairs ECM-induced EC motility and migration independently of VEGFR2 in a pathway that is conserved between mice and humans.

Identification of NRP1-dependent, ECM-induced signal transduction pathways

Because FN stimulation activated NRP1-dependent actin remodeling and cell migration independently of VEGF165 and VEGFR2, we sought to identify candidate effectors with a phosphokinase antibody array (e.g., Zhuang et al., 2012). For this experiment, HDMECs were transfected with si-NRP1 or control siRNA (Fig. 2 A), and then serum-starved and stimulated with VEGF165 (Fig. 2 B) or plated on FN (Fig. 2 C). We observed reduced VEGF165-induced activation of the MAPK p38 in ECs lacking NRP1, as expected (Kawamura et al., 2008), and additionally impaired FN-induced P38 activation in ECs lacking NRP1 (Fig. 2, B and C). The screen also showed that NRP1 down-regulation in VEGF165-stimulated HDMECs reduced AKT activation (Fig. 2 B), as previously reported for HUVECs (Pan et al., 2007a,b; Koch et al., 2011). Unexpectedly, however, NRP1 down-regulation did not impair AKT phosphorylation in FN-stimulated ECs (Fig. 2 C).

Consistent with findings in HUVECs and zebrafish (Lanahan et al., 2010, 2013), NRP1 loss decreased both VEGF165- and FN-induced activation of PLCγ1 (Fig. 2, B and C), known to promote the phosphorylation of the focal adhesion protein PXN downstream of FN-mediated integrin activation to increase cell spreading and migration (Choi et al., 2007; Zaidel-Bar et al., 2007). Consistent with reduced

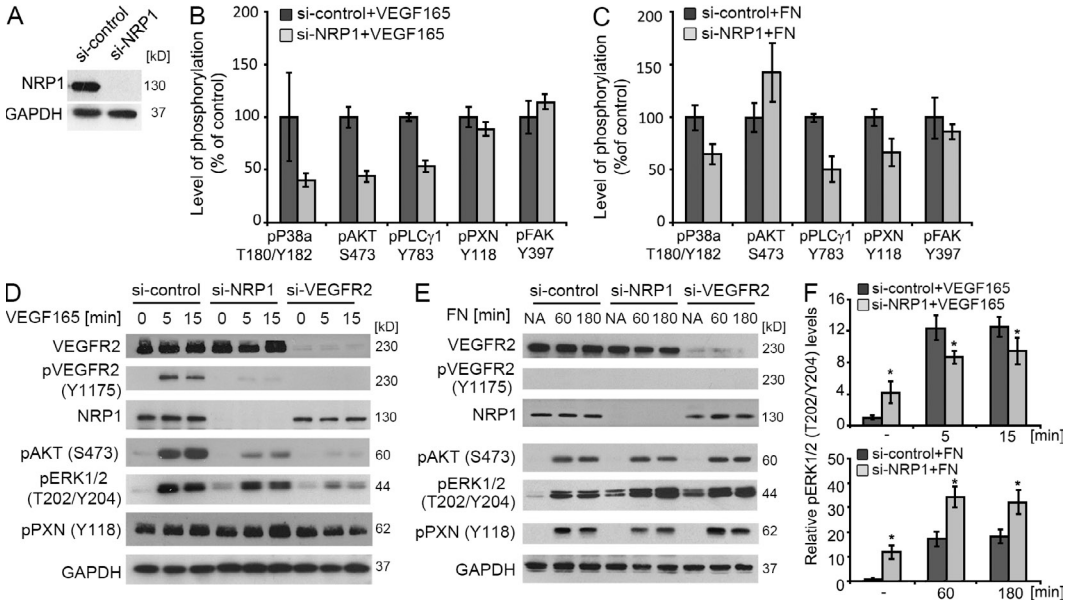

Figure 2. NRP1 transduces ECM signals independently of VEGF165 and VEGFR2. (A–C) For phosphoproteomic screening, HDMECs were transfected with control or NRP1 siRNA before immunoblotting to confirm NRP1 knockdown (A) or stimulation with VEGF165 for 10 min (B) or FN for 30 min (C), followed by phosphokinase-antibody array screening. Phosphorylation of the indicated proteins in si-NRP1 relative to si-control transfected cells from 2 independent experiments, performed in duplicate each, were shown as mean fold change ± SEM. (D and E) To validate NRP1-regulated phosphoproteins identified in the phosphoproteomic screen, HDMECs were transiently transfected with control, NRP1 or VEGFR2 siRNA and stimulated with VEGF165 (D) or plated on FN (E) for the indicated times. Lysates were immunoblotted for the indicated proteins, with GAPDH serving as a loading control. Immunoblots are representative of 3 independent experiments. (F) pERK (T202/Y204) levels were quantified as pixel intensity relative to GAPDH and values expressed as mean fold change ± SEM. *, $P < 0.05$, Student's *t* test.

PLCγ1 activation and a requirement for NRP1 in integrin ligand-mediated EC spreading and motility, PXN phosphorylation on tyrosine residue (Y) 118 was also reduced in FN-stimulated HDMECs lacking NRP1 (Fig. 2 C). In contrast, VEGF165-induced PXN phosphorylation was unaffected by NRP1 loss (Fig. 2 B). Loss of NRP1 did not affect the phosphorylation of FAK on residue Y397 downstream of either VEGF or FN (Fig. 2 B). This was unexpected, as phosphorylation of this residue activates FAK kinase, which is then able to phosphorylate PXN (Chen et al., 1996; Parsons et al., 2000). Collectively, the phosphoantibody screen indicated essential and distinct roles for NRP1 in VEGF165- versus ECM-stimulated signal transduction and suggested that NRP1 promotes PXN phosphorylation downstream of ECM activation independently of VEGFR2 or FAK.

Differential dependency of ECM signaling pathways on NRP1 and VEGFR2

Immunoblotting validated the results from the phosphoantibody screen and allowed us to more directly compare NRP1 and VEGFR2 dependence of specific signal transduction pathways (Fig. 2, D and E). For these experiments, HDMECs were serum-starved and plated on FN or grown on tissue culture plastic, serum-starved, and then stimulated with VEGF165. As expected, VEGF165-induced VEGFR2 phosphorylation was inhibited by NRP1 or VEGFR2 downregulation (Fig. 2 D). In contrast, FN stimulation did not induce comparable VEGFR2 stimulation (Fig. 2 E). Also as expected, NRP1 or VEGFR2 knockdown decreased VEGF165-induced AKT phosphorylation; however, FN-induced AKT phosphorylation was unaffected by NRP1 or VEGFR2 deficiency (Fig. 2, D and E). The AKT pathway therefore transduces growth factor but not ECM signals in a VEGFR2- and NRP1-dependent fashion. Agreeing with experiments in other types of ECs (Pan et al., 2007a; Lanahan et al., 2010; Ren et al., 2010), VEGF165-induced ERK1/2 phosphorylation was impaired after NRP1 or VEGFR2 knockdown in HDMECs (Fig. 2, D and F). Surprisingly, however, ERK1/2 phosphorylation was significantly increased in response to FN (Fig. 2, E and F). Finally, we used immunoblotting to examine how NRP1 and VEGFR2 knockdown affected PXN tyrosine phosphorylation. Although NRP1 loss reduced PXN phosphorylation in FN-stimulated HDMECs, VEGFR2 knockdown did not (Fig. 2 E). In contrast, PXN was constitutively phosphorylated in adherent HDMECs, with phosphorylation increasing slightly after VEGF165 stimulation in a VEGFR2-dependent manner (Fig. 2 D; Birukova et al., 2009), but NRP1 was not required for VEGF165-induced PXN phosphorylation (Fig. 2 D). Together with the phosphoantibody screen, these findings demonstrate that ECM- and VEGF165-induced signal transduction pathways are differentially affected by NRP1 loss, and that NRP1-dependent PXN phosphorylation occurs independently of VEGFR2.

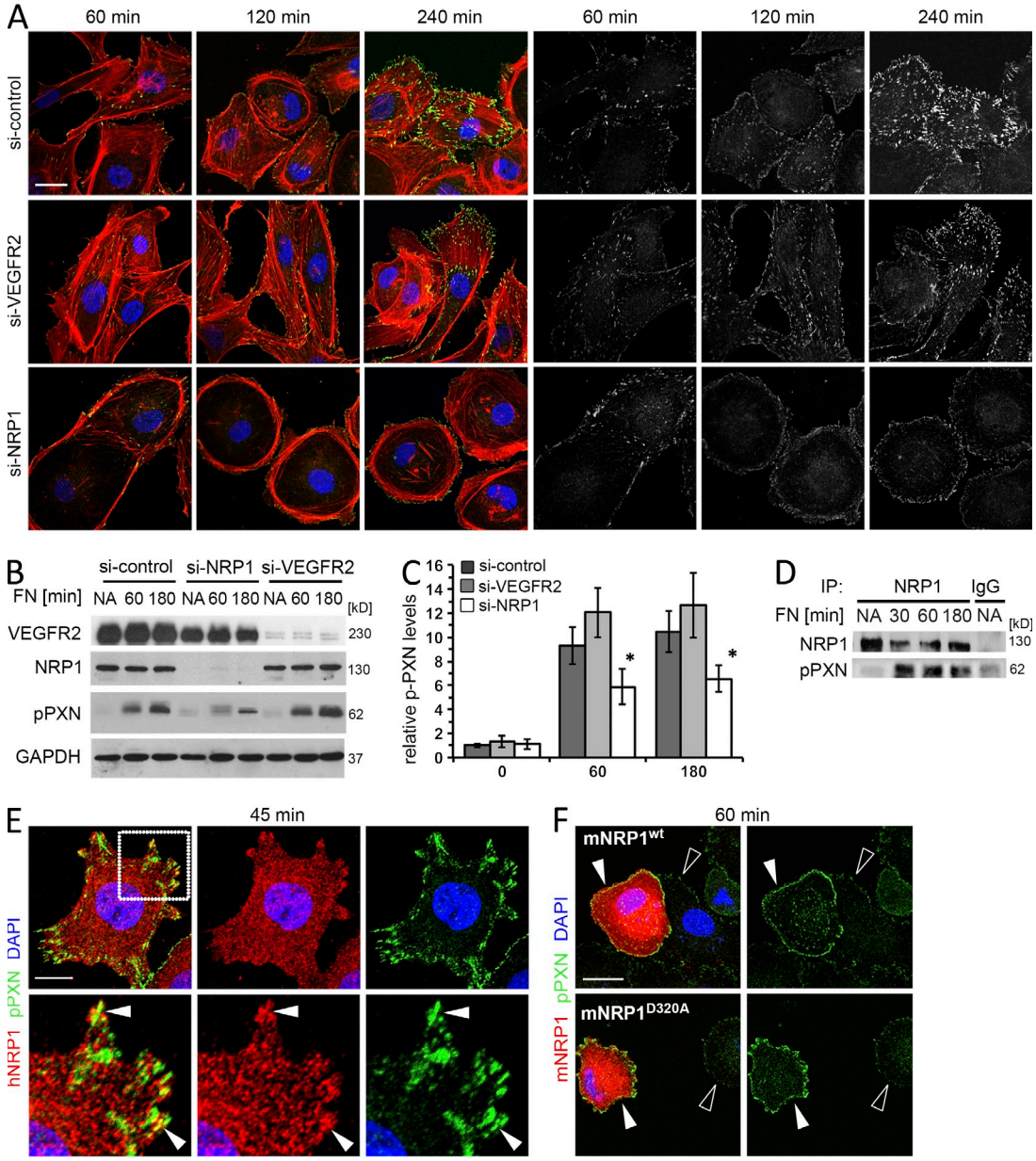

Figure 3. NRP1 promotes FN-induced PXN Y118 phosphorylation. (A and B) HDMECs transiently transfected with control, NRP1 or VEGFR2 siRNA were plated on FN for the indicated times and immunofluorescently labeled (A) for pPXN Y118 (green) together with phalloidin (red) and DAPI (blue; bar, 20 µm) or immunoblotted for the indicated proteins (B). The single channel for pPXN staining is shown on the right side of A. (C) pPXN Y118 levels in immunoblots from 4 independent experiments were quantified as pixel intensity relative to GAPDH and values expressed as mean fold change ± SD in si-VEGFR2 or si-NRP1 relative to control siRNA transfected cells. *, $P < 0.05$, Student's *t* test. (D) To examine if NRP1 forms a complex with pPXN in FN-stimulated ECs, HDMECs were detached in serum-free medium (nonadherent, NA) or plated on FN for the indicated times and then immunoprecipitated with control IgG or NRP1 antibodies, followed by immunoblotting for NRP1 and pPXN Y118. The immunoblot is representative of 4 independent experiments. (E) Single confocal scans of HDMECs plated on FN for 45 min and then immunofluorescently labeled with antibodies specific for human NRP1 or pPXN Y118 and counterstained with DAPI. Bar, 10 µm. A higher magnification of the area indicated with a dotted square is shown in the bottom row, and single channels for NRP1 and pPXN are shown adjacent to the triple stains at low and high magnification. Arrowheads indicate examples of partial colocalization. (F) HDMECs were transfected with pCDNA3.1 encoding wild-type mouse NRP1 or mutant mouse NRP1^{D320A}, plated on FN for 60 min, and then labeled with antibodies specific for mouse NRP1 and pPXN and counterstained with DAPI. The single channel for pPXN staining is shown on the right. Cells expressing murine NRP1 (white arrowheads) up-regulate pPXN. Note that the antibody does not detect endogenous human NRP1 in untransfected cells (clear arrowheads). Bar, 20 µm.

NRP1, not VEGFR2, is required for ECM-induced PXN phosphorylation and focal adhesion localization

Because pPXN is recruited to focal adhesions to promote their turnover during cell migration (Zaidel-Bar et al., 2007; Pasapera et al., 2010) and NRP1-deficient ECs have reduced pPXN (Figs. 1 and 2), we examined NRP1-dependent pPXN localization in FN-stimulated HDMECs by immunostaining. In control cells, pPXN increased over time and was present in

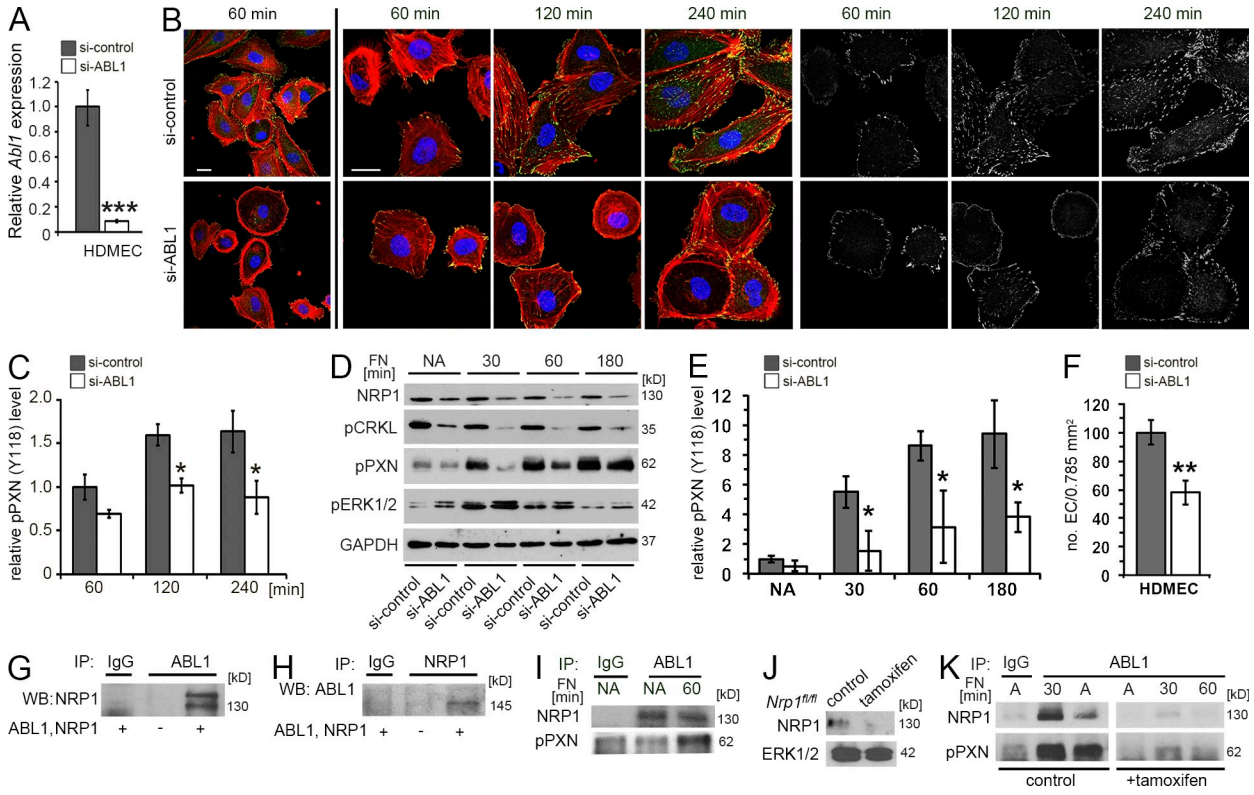

Figure 4. ABL1 knockdown impairs PXN Y118 phosphorylation and EC migration. (A) qPCR analysis for *Abl1* expression in HDMECs. *Abl1* values were normalized to *Actb* and expressed as fold reduction in knockdown relative to control HDMECs (mean ± SD of 3 independent experiments). ***, $P < 0.001$, Student's *t* test. (B–E) Immunofluorescence labeling (B and C) and immunoblotting (D and E) of HDMECs transfected with si-ABL1 or control siRNA and then plated on FN for the indicated times. In B, pPXN Y118 (green) is shown together with phalloidin (red) and DAPI (blue) on the left, and as single channel in grayscale on the right. Bars, 20 µm. The pixel intensity of the pPXN signal was quantified in C as fold change in knockdown cells at the indicated time points relative to control cells at 60 min (mean ± SEM of 4 independent experiments). *, $P < 0.05$, Student's *t* test. (D and E) Immunoblotting shows that ABL1 down-regulation reduces PXN, but not ERK1/2 phosphorylation. pCRKL served as readout for ABL1 down-regulation and GAPDH as a loading control. The quantitation of pPXN Y118 levels as pixel intensity after densitometry is shown in E. Values are expressed as fold change in knockdown cells at the indicated time points relative to nonadherent (NA) control cells at 0 min (mean ± SD of 3 independent experiments). *, $P < 0.05$, Student's *t* test. (F) HDMECs transfected with control or ABL1 siRNA were plated on FN-coated transwells and the percentage of transmigrated HDMECs determined after 240 min in knockdown relative to control cells (mean ± SEM in 4 independent experiments). **, $P < 0.01$, Student's *t* test. (G and H) To investigate if ABL1 and NRP1 form a constitutive protein complex in ECs and associate with pPXN in FN-stimulated cells, HEK cells were transfected with expression vectors for NRP1 and ABL1 (+) before immunoprecipitation with control IgG or ABL1 antibody and immunoblotting for NRP1 (G), or immunoprecipitation with NRP1 and immunoblotting for ABL1 (H). Nontransfected cells (−) were used as internal negative control. (I) To examine complex formation of endogenous NRP1, ABL1, and pPXN, HDMECs were detached and lysed (nonadherent, NA) or lysed after plating on FN for the indicated times. Lysates were immunoprecipitated with control IgG or ABL1 antibody followed by immunoblotting for NRP1 and pPXN Y118. (J and K) To examine if ABL1 recruits pPXN in a NRP1-dependent manner after FN stimulation, neonatal *Nrp1*$^{fl/fl}$ mice were induced with vehicle (control) or tamoxifen to delete NRP1 (J) and isolated MLECs cultured on FN before being detached and lysed (A) or lysed after plating on FN for the indicated times. Lysates were immunoprecipitated with IgG or ABL1 antibody and immunoblotted for NRP1 and pPXN Y118 (K).

focal adhesions at the end of F-actin stress fibers, correlating with an elongated cell shape (Fig. 3 A). FN-stimulated HDMECs, therefore, displayed the hallmarks of polarized cells. Although VEGFR2 down-regulation did not impair these responses, HDMECs lacking NRP1 displayed their characteristic rounded morphology with abundant cortical actin; correlating with the lack of stress fibers, pPXN levels were significantly decreased, with remaining pPXN being localized mainly to the cell periphery (Fig. 3, A and B). Immunoblotting established that siRNA targeting had been effective and further confirmed reduced pPXN in NRP1-deficient cells (Fig. 3 B); in contrast, pPXN was slightly but significantly increased in VEGFR2-deficient cells (Fig. 3, B and C). These findings demonstrate that NRP1 promotes PXN phosphorylation in a VEGFR2-independent fashion.

Because both the phosphoantibody screen and immunoblotting suggested a functional relationship between NRP1 and pPXN, we examined if both proteins interact. In agreement, NRP1 immunoprecipitation, followed by pPXN immunoblotting, demonstrated an FN-dependent interaction in HDMECs (Fig. 3 D). Moreover, immunofluorescence showed partial colocalization in peripheral cell areas resembling focal adhesions (Fig. 3, E and F). The finding that NRP1 and pPXN associate in FN-stimulated ECs agrees with a study showing

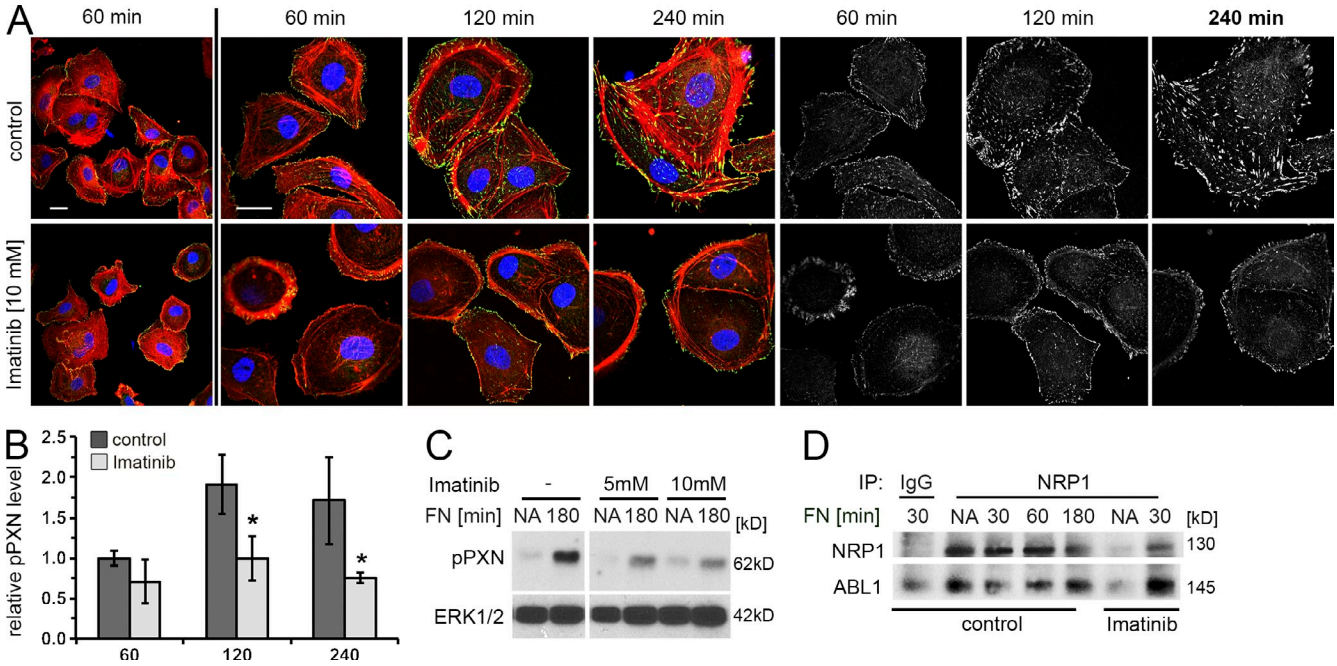

Figure 5. ABL1 kinase activity is essential for PXN Y118 phosphorylation in HDMECs in vitro. (A–C) To examine if ABL1 kinase activity is essential for PXN phosphorylation, we performed immunofluorescence labeling (A and B) and immunoblotting (C) of HDMECs treated with vehicle or Imatinib 30 min before and during plating on FN for the indicated times. In A, pPXN Y118 (green) is shown together with phalloidin (red) and DAPI (blue) on the left and as single channel in grayscale on the right. Bars, 20 µm. pPXN pixel intensity was quantified in B and expressed as fold change in knockdown cells at the indicated time points relative to control cells at 60 min (mean ± SD of 4 independent experiments). *, $P < 0.05$, Student's *t* test. (C) Immunoblotting confirmed that Imatinib treatment reduced pPXN Y118 levels. Total ERK1/2 levels were used as a loading control. (D) To examine if endogenous NRP1 and ABL1 form a complex in ECs, we performed coimmunoprecipitation of endogenous proteins from lysates of HDMECs, treated with vehicle or 10 µM Imatinib for 30 min, detached, and plated on FN for the indicated times in the presence of Imatinib. Immunoprecipitation using ABL1 antibody was followed by immunoblotting performed for NRP1 and ABL1.

that overexpressed NRP1 colocalizes with α5β1 integrins at endothelial adhesion sites (Valdembri et al., 2009).

To examine the relationship between NRP1 and pPXN in a gain-of-function experiment, we transfected a construct encoding murine NRP1 into HDMECs and validated NRP1 overexpression with an antibody specific for murine NRP1 (Fig. 3 F). This experiment demonstrated increased PXN phosphorylation after FN stimulation in transfected compared with neighboring untransfected cells (Fig. 3 F, top). Importantly, overexpressing a VEGF165 binding-deficient NRP1 mutant ($mNRP1^{D320A}$; Herzog et al., 2011) similarly increased PXN phosphorylation (Fig. 3 F, bottom), confirming that FN/NRP1-dependent pPXN induction does not depend on VEGF binding to NRP1. Collectively, these results establish that NRP1 regulates PXN phosphorylation independently of VEGF.

ABL1 is essential for ECM-induced PXN phosphorylation

Because NRP1 lacks catalytic activity, it requires a partner kinase to promote FN-induced PXN phosphorylation, but this kinase is not VEGFR2 (Fig. 1) or FAK (Fig. 2, B and C). A good candidate is the cell adhesion–associated kinase ABL1, which interacts with PXN in FN-stimulated fibroblasts (Lewis and Schwartz, 1998) as well as integrins β1 and β2 (Cui et al., 2009; Baruzzi et al., 2010). Furthermore, the Y118 residue that is phosphorylated in an NRP1-dependent fashion resides in an ABL1 phosphorylation consensus site (Cujec et al., 2002), and ABL1 is an effector of NRP1 and integrins in tumor matrix remodeling (Yaqoob et al., 2012). To investigate ABL1 function in FN-stimulated ECs, we used two independent but complementary methods: siRNA-mediated knockdown of ABL1 (Fig. 4) and pharmacological inhibition of ABL1 kinase activity (Fig. 5).

ABL1 knockdown was achieved by transfecting HDMECs with control siRNA or siRNA targeting ABL1 (si-ABL1) and confirmed by qPCR (Fig. 4 A). We found that targeting ABL1 caused a phenotype similar to NRP1 knockdown. Thus, immunostaining revealed significantly reduced pPXN levels, with residual pPXN accumulating in the cell periphery (Fig. 4, B and C). Moreover, there was a conspicuous absence of pPXN-positive focal adhesion contacts and stress fibers, but abundant cortical actin, correlating with impaired cell spreading and a round rather than elongated cell shape, as observed after NRP1 knockdown (Fig. 4 B). Immunoblotting for the phosphorylated form of the ABL1 target CRKL (Lewis et al., 1996) confirmed ABL1 down-regulation as well as significantly reduced FN-stimulated pPXN in ABL1 knockdown compared with control cells (Fig. 4, D and E).

This analysis also showed increased ERK1/2 phosphorylation after ABL1 knockdown (Fig. 4 D), similar to NRP1 knockdown (Fig. 2, E and F). Unexpectedly, NRP1 protein expression also decreased in a time-dependent manner after ABL1 knockdown (Fig. 4 D), but this decrease was not caused by reduced *NRP1* mRNA levels (si-ABL1 relative to si-control: 1.18 ± 0.13 at 0 min; 1.17 ± 0.11 at 30 min; 1.07 ± 0.07 at 60 min; mean ± SD; $n = 3$; $P > 0.05$). ABL1 therefore positively regulates NRP1 protein stability in HDMECs in response to FN stimulation. Hence, ABL1 may affect NRP1-dependent pPXN up-regulation in a dual fashion, first by directly promoting PXN phosphorylation, and second by stabilizing NRP1 protein and therefore increasing the capacity of HDMECs to respond to FN and up-regulate PXN phosphorylation via an NRP1-dependent pathway.

Because PXN phosphorylation promotes the turnover of focal adhesions that serve as traction points during cell migration (Zaidel-Bar et al., 2007), we predicted that ABL1 loss would impair EC migration on FN. In agreement, a transwell assay showed a 40% reduction in haptotactic migration after ABL1 knockdown (Fig. 4 F), which was similar to the reduction observed after NRP1 knockdown (Fig. 1, K and L). NRP1 and ABL1 therefore similarly regulate PXN phosphorylation, actin remodeling, and cell migration in FN-stimulated ECs.

ABL1 forms a complex with NRP1 in ECs

The similar cellular changes caused by ABL1 and NRP1 deficiency raised the possibility that both proteins interact to regulate PXN phosphorylation. To investigate this idea, we cotransfected HEK293 cells with expression constructs for NRP1 and ABL1. ABL1 immunoprecipitation followed by NRP1 immunoblotting, and vice versa, showed that both proteins formed a complex (Fig. 4, G and H). Immunoprecipitating ABL1 from HDMECs followed by NRP1 immunoblotting confirmed the existence of an endogenous complex and further showed that this complex had recruited pPXN 60 min after FN stimulation (Fig. 4 I). To investigate whether this complex also forms in murine ECs, we inactivated two conditional *Nrp1*-null alleles in newborn mice with a tamoxifen-inducible endothelial *Cre* transgene (Fantin et al., 2013) and then isolated ECs (Fig. 4 J). As observed for HDMECs, ABL1 immunoprecipitated NRP1 in control MLECs adhering to FN, and complex formation was increased after detaching the cells and plating them for 30 min on FN (Fig. 4 K). Moreover, pPXN was present in the ABL1–NRP1 complex of MLECs from both conditions (Fig. 4 K), as seen in HDMECs (Fig. 4 I). In contrast, NRP1 was not immunoprecipitated effectively in MLECs from tamoxifen-treated mice, and complex formation of ABL1 with pPXN was reduced (Fig. 4 K). These data demonstrate that ABL1 and NRP1 form a complex and that ABL1 recruits pPXN in an NRP1-dependent fashion.

ABL1 kinase inhibition reduces ECM-induced PXN phosphorylation

To examine if ABL1 kinase activity was required for FN-induced PXN phosphorylation, we treated HDMECs with Imatinib (Glivec), a small molecule inhibitor that effectively targets ABL1 but not VEGFR2 (Buchdunger et al., 2002; Anselmi et al., 2012) and has been approved for therapy in cancers with up-regulated ABL1 kinase activity (Druker et al., 1996). As observed in si-ABL1–transfected cells, Imatinib-treated HDMECs formed few stress fibers, but abundant cortical actin, and they adopted a round shape with reduced cell spreading; moreover, they had low pPXN phosphorylation, with residual pPXN in the cell periphery rather than in areas where stress fibers normally terminate in focal adhesions (Fig. 5 A). The quantitation of pixel intensities in immunostains (Fig. 5 B) and immunoblots (Fig. 5 C) confirmed significantly reduced PXN phosphorylation in Imatinib-treated compared with control cells. NRP1 immunoprecipitation of Imatinib-treated HDMECs followed by ABL1 immunoblotting showed that both proteins formed a complex before FN stimulation, independently of ABL1 kinase activity (Fig. 5 D). We conclude that ABL1 stimulates PXN phosphorylation in an NRP1-dependent fashion when ECs migrate on FN.

NRP1 regulates ABL1–mediated PXN phosphorylation in retinal angiogenesis

To examine if NRP1 and ABL1 also promote PXN phosphorylation in an ECM-dependent angiogenesis model in vivo, we studied the perinatal mouse retina; in this organ, endothelial sprouts headed by filopodia-studded tip cells migrate toward astrocyte-localized VEGF in the retinal periphery, with filopodia being guided by astrocyte-derived FN (Fig. 6 A; Ruhrberg et al., 2002; Gerhardt et al., 2003; Stenzel et al., 2011). Immunostaining confirmed FN deposition around IB4-stained vessels and ahead of the vascular front in a fine meshwork characteristic of astrocytes (Fig. 6 B). To investigate how NRP1 deficiency affected pPXN levels during retinal angiogenesis, we could not use $Nrp1^{-/-}$ mice, as they die before birth (Kawasaki et al., 1999). Instead, we compared $Nrp1^{+/+}$ and $Nrp1^{+/-}$ littermates because the latter are viable but nevertheless have mild angiogenesis defects (Fantin et al., 2013). Immunoblotting confirmed significantly decreased NRP1 levels in P6 $Nrp1^{+/-}$ mice (Fig. 6 C). Single optical slices, acquired by confocal microscopy after immunolabeling, revealed pPXN staining in ECs at the IB4-positive vascular front, including tip cells and their filopodia, and also some pPXN ahead of the vascular front (Fig. 6 D). As observed for si-NRP1–targeted HDMECs, pPXN staining appeared reduced in $Nrp1^{+/-}$ littermates, both in vascular and avascular areas (Fig. 6 D). To confirm that this defect was cell autonomous in vascular endothelium, we also used *Cre-LoxP* recombination approach to delete NRP1 (Fig. 1). Thus, conditional *Nrp1*-null mice lacking or expressing a tamoxifen-inducible, endothelial-specific *Cre* transgene were treated with tamoxifen from postnatal day 2 (P2) to P5 and stained for IB4 and pPXN. As seen in $Nrp1^{+/-}$ mice, tamoxifen-treatment reduced pPXN in *Cre*-expressing but not *Cre*-negative (control) littermates (Fig. 6 D).

To quantify pPXN specifically in ECs, we isolated IB4-positive areas by applying a virtual mask over IB4-negative

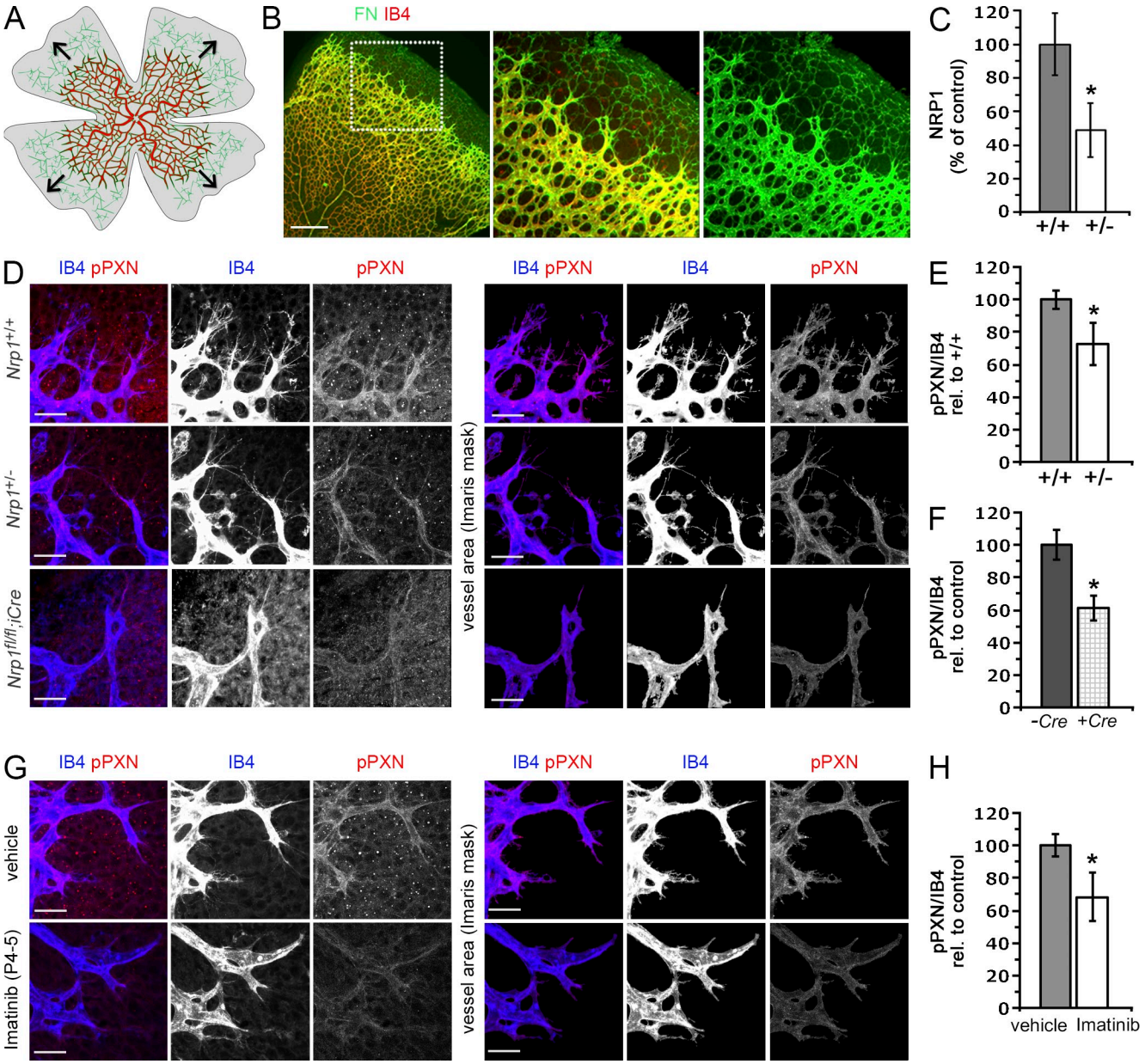

Figure 6. NRP1 and ABL1 promote PXN phosphorylation during retinal angiogenesis in the mouse. (A) A schematic representation of retinal angiogenesis illustrates how vessels (red) expand from the retinal center toward the periphery (indicated by arrows). Vessels are guided by an astrocyte-derived FN network (green) ahead of the vascular front, but FN subsequently overlaps partially with the vessel pattern (red with green outline). (B) Immunolabeling for FN together with the vascular marker IB4 demonstrates angiogenesis in the P6 retina. Bar, 400 µm. The area shown in higher magnification is indicated with a dotted square in the first panel. (C) Reduced NRP1 levels in *Nrp1*$^{+/-}$ compared with *Nrp1*$^{+/+}$ littermates, shown by immunoblot quantification of NRP1 protein levels in P6 lungs. NRP1 levels were normalized to VE-cadherin levels and expressed as percentage relative to wild type (mean ± SEM; $n \geq 3$). *, $P < 0.05$, Student's *t* test. (D–H) Single confocal slices through the vascular front in retinas of *Nrp1*$^{+/+}$, *Nrp1*$^{+/-}$ littermate mice and tamoxifen-inducible EC-specific *Nrp1*-null mice injected with tamoxifen from P2 to P5 (D) or treated with vehicle or 100 mg/kg/d Imatinib on days P4 and P5 (G). Retinas were immunostained for pPXN Y118 and IB4. Bar, 15 µm. In D and G (right), Imaris software was used to mask areas not labeled for IB4 to reveal pPXN staining in ECs. Quantification of vascular pPXN in optical z-stacks after applying a mask to isolate IB4-positive areas in *Nrp1*$^{+/-}$ (E), tamoxifen-inducible EC-specific *Nrp1*-null mutants (F), and Imatinib-treated mice (H) relative to controls. Mean pixel values of pPXN relative to IB4 are expressed as percentage of control ± SEM ($n = 3$). *, $P < 0.05$, Student's *t* test.

areas (Fig. 6 D, right). Quantification of pPXN relative to IB4 pixel intensity in masked 3D projections of z-stacks showed significantly reduced endothelial pPXN staining at the vascular front of heterozygous *Nrp1*-null mutants (Fig. 6 E) and endothelial-specific *Nrp1*-null mutants (Fig. 6 F) compared with controls.

To examine if ABL1 was also required for PXN phosphorylation in retinal ECs, we treated neonates with Imatinib or vehicle (Fig. 6, G and H). Single confocal slices showed that pPXN staining was reduced in P6 retinas after 2 days of treatment (Fig. 6 G), as observed for NRP1 mutants. To quantify pPXN specifically in ECs, we again isolated IB4-positive areas with a virtual mask (Fig. 6 G, right) and found that endothelial pPXN pixel intensity was significantly reduced after Imatinib treatment (Fig. 6 H). ABL1 therefore promotes PXN phosphorylation in angiogenic ECs in vivo, similar to NRP1 and as observed for FN-stimulated ECs in vitro.

ABL1 activation is essential for physiological angiogenesis in the retina

Because ABL1 is involved in NRP1-mediated actin remodeling, cell migration, and PXN phosphorylation, we investigated next if it is also essential for blood vessel growth in vivo. IB4 labeling showed reduced vascular extension and network density in retinal flat mounts of P6 Imatinib-treated compared with vehicle-treated mice (Fig. 7 A). Quantitation confirmed a small but significant reduction in vascular extension across the retina (Fig. 7 B), as previously reported for loss of astrocyte FN (Stenzel et al., 2011). In agreement, FN immunostaining showed reduced astrocyte FN deposition ahead of the vascular front (Fig. 7, C and D), likely due to Imatinib targeting of PDGFR signaling in astrocytes (Buchdunger et al., 2002). In contrast, we observed abundant FN deposition around retinal vessels in both control and Imatinib-treated mice, with no difference in FN pixel intensity in IB4-positive areas (Fig. 7, C and D). Vascular FN assembly was therefore not compromised by ABL1 targeting.

High magnification images of the retinal vascular front in control and Imatinib-treated mice showed that vessels had sprouted and formed numerous tip cell filopodia (Fig. 7 E), consistent with the concept that VEGF gradients rather than matrix pathways drive these processes (Ruhrberg et al., 2002; Gerhardt et al., 2003). However, sprouts in Imatinib-treated mice appeared longer and wider, with fewer lateral protrusions connecting to neighboring sprouts (Fig. 7, E and F, arrows), and filopodia often appeared thin, wavy, and misoriented (Fig. 7 E, arrowheads). This phenotype agrees with a role for the NRP1–ABL1 complex in endothelial actin remodeling (Fig. 1). Moreover, the filopodia defects resemble those previously seen at the retinal vascular front of mice with a genetic lack of astrocyte FN (Stenzel et al., 2011). Yet loss of astrocyte FN in itself does not impair vessel sprouting and branching (Stenzel et al., 2011), suggesting that the more severe vascular defects of Imatinib-treated retinas are due to an EC-autonomous role for ABL1.

To further define the vascular defects caused by ABL1 inhibition, we compared vessel sprouting and branching in mice treated with Imatinib for different times (Fig. 7, F and G). Quantitative analysis revealed significantly fewer tip cells, defined by the presence of filopodial bursts at the vascular front (Fig. 7 G). Consistent with reduced tip cell density and impaired lateral sprout extension, we also observed a significant and Imatinib dose-dependent reduction in branch points behind the vascular front, indicative of reduced sprout fusion (Fig. 7 G). These findings therefore agree with the recently shown requirement of actin-based filopodia dynamics for sprout fusion and therefore vascular network formation (Phng et al., 2013).

Because our data suggest that ABL1 is involved in NRP1-mediated angiogenic processes, we also compared the retinal vascular phenotype of Imatinib-treated mice to that of endothelial-specific *Nrp1* mutants. For this experiment, we treated *Cre*-positive and *Cre*-negative littermates with tamoxifen in a regimen similar to that used for Imatinib. We observed a significant reduction in both tip cell density and vascular branch points in mutants, similar to Imatinib-treated mice (Fig. 7 G).

Based on the in vitro and in vivo data we have described here, we conclude that NRP1 facilitates angiogenesis in response to integrin ligands via ABL1-mediated PXN phosphorylation and actin remodeling. Because this pathway operates independently of VEGF and VEGFR2, NRP1 plays a dual role in angiogenesis and vascular morphogenesis by independently promoting ECM-stimulated and growth factor–induced signals in ECs (Fig. 7 H). In agreement, vascular extension is more severely inhibited in EC-specific *Nrp1* knockout compared with Imatinib-treated retinas (reduction in vascular extension compared with littermate controls: 32 ± 4% for endothelial *Nrp1* knockouts vs. 14 ± 1% for Imatinib-treated mice).

Imatinib treatment decreases pathological angiogenesis

To assess the relevance of the FN-induced NRP1–ABL1 pathway for pathological vessel growth, we used a mouse model of oxygen-induced retinopathy (OIR; Connor et al., 2009). In this model, the sequential exposure of mouse pups to hyperoxia followed by normoxia leads to the formation of retinal neovascular lesions that resemble those observed in PDR patients and in babies with ROP, which arises after moving them out of incubators with high oxygen tension (Connor et al., 2009). Specifically, the exposure of neonatal mice to hyperoxia from P7 to P12 induces vasoobliteration of central retinal capillaries, which causes central retinal hypoxia on return to room air. The ensuing up-regulation of VEGF and other proangiogenic factors then activates angiogenesis, but this process fails to effectively revascularize the retina and instead leads to abundant tuft-like vascular malformations that protrude into the vitreous (Smith et al., 1994). Immunostaining of flat-mounted retinas on P17, 5 days after return to room air, showed that these neovascular tufts were FN positive (Fig. 8 A), suggesting that OIR is a suitable model to examine the role of NRP1 and ABL1 in ECM-mediated angiogenesis pathways. In agreement, Imatinib treatment of mouse pups from their return to normoxia until P17 significantly reduced revascularization of avascular areas (AV; Fig. 8, B and C) and effectively inhibited the formation of neovascular tufts (Fig. 8, B–D).

In agreement with ABL1 acting downstream of NRP1, a reduction in both revascularization of avascular areas and neovascular tuft formation was also seen in conditional endothelial

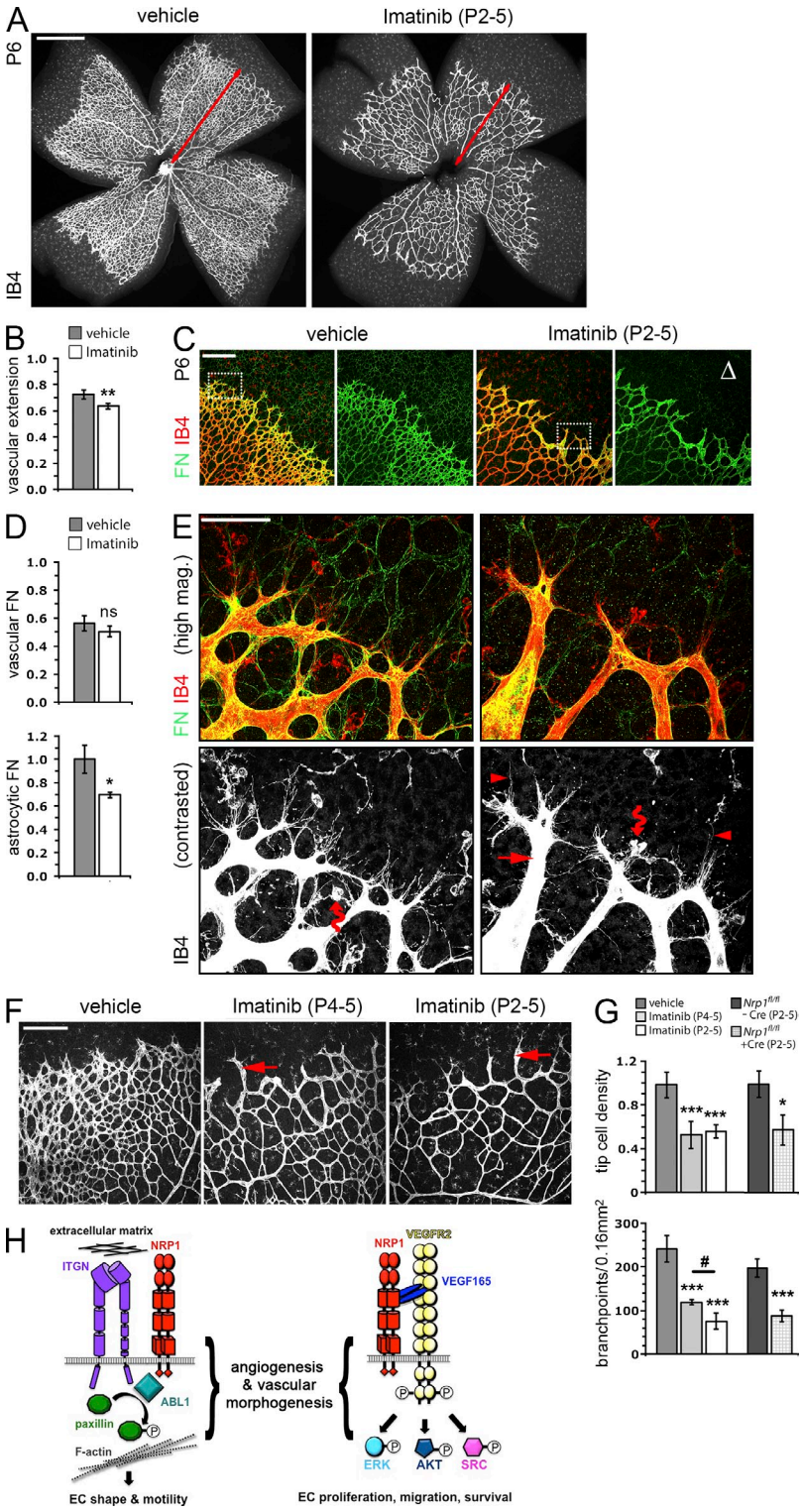

Figure 7. ABL1 is essential for vessel spouting and branching in the retina. (A and B) P6 retinal vasculature of mice treated with vehicle or Imatinib from P2 to P5 was immunolabeled for IB4. Bar, 1 mm. Vascular extension from the retinal center to the vascular front is indicated with red arrows. (B) Vascular extension after Imatinib treatment was quantified as the distance of the IB4-positive front from the retinal center relative to the retinal radius (vehicle, $n = 7$ mice; Imatinib, $n = 4$ mice; **, $P < 0.01$, Student's t test). Error bars show SD. (C–E) P6 retinal vasculature of mice treated with vehicle or Imatinib from P2 to P5 was immunolabeled for IB4 and FN. Bars: (C) 200 µm; (E) 50 µm. Note reduced FN staining of astrocyte processes ahead of the vascular front (Δ), whereas the vasculature was prominently stained for FN. (D) Quantification of FN pixel intensity in Imatinib-treated retinas in 0.06-mm² areas of astrocyte networks ahead of the vascular front (fold change compared with controls; $n = 3$ mice each; *, $P < 0.05$, Student's t test) and in vascular areas, isolated with an IB4-guided IMARIS mask (FN relative to IB4 pixel intensity; $n = 3$ mice each; $P > 0.05$, Student's t test). Error bars show SD. Higher magnification of the areas indicated with dotted squares in C demonstrates abnormal filopodia and sprout morphology in Imatinib-treated retinas. The IB4 single channel is shown in grayscale below each panel after contrast enhancement to highlight filopodia. The arrow indicates an abnormally long and wide sprout without lateral protrusions or connections. Examples of abnormally thin, wavy, and misoriented filopodia are indicated with arrowheads. Note that the interaction of tip cells with microglia (wavy arrow) is not prevented by Imatinib treatment. (F and G) IB4-labeled P6 retinal vasculature of mice treated with vehicle or Imatinib by daily injections on P4 and P5 or from P2 to P5. Bar, 200 µm. Examples of abnormally long and wide sprouts without lateral protrusions or connections are indicated with arrows. (G) Quantification of filopodial bursts per vascular front length as an indicator of tip cell number, and quantification of branch points behind the vascular front (vehicle, $n = 7$ mice, vs. Imatinib P4-5, $n = 3$ mice, or Imatinib P2–5, $n = 4$ mice; ***, $P < 0.001$ vs. vehicle control, ANOVA with Tukey's comparison test; #, $P < 0.05$ for P4–5 vs. P2–5 treatment, Student's t test; P2–5 tamoxifen-injected *Nrp1*$^{fl/fl}$ mice lacking *Cre*, $n = 8$, or expressing *Pdgfb-iCre-ERT2-Egfp*, $n = 6$; *, $P < 0.05$; ***, $P < 0.001$ versus control, Student's t test). Error bars show SD. (H) Schematic representation of the NRP1–ABL1–PXN pathway and its synergism with known VEGF signaling pathways transduced by VEGFR2.

Nrp1-null mutants treated with a tamoxifen regimen analogous to that used for Imatinib treatment (Fig. 8, E and F). Even though the vascular OIR phenotype of *Nrp1* mutants was similar to that of Imatinib-treated mice, the reduction in neovascular growth was greater, consistent with a dual role for NRP1 in ECM-stimulated ABL1 and VEGF-induced VEGFR2 pathways in postnatal angiogenesis (reduction in neovascular tuft formation compared with littermate controls: 60 ± 13% for endothelial *Nrp1* knockouts vs. 28 ± 10% for Imatinib-treated mice; Fig. 7 H).

Finally, we assessed the efficacy of Imatinib in targeting angiogenesis in the ear wound healing model (Fig. 8 G), in

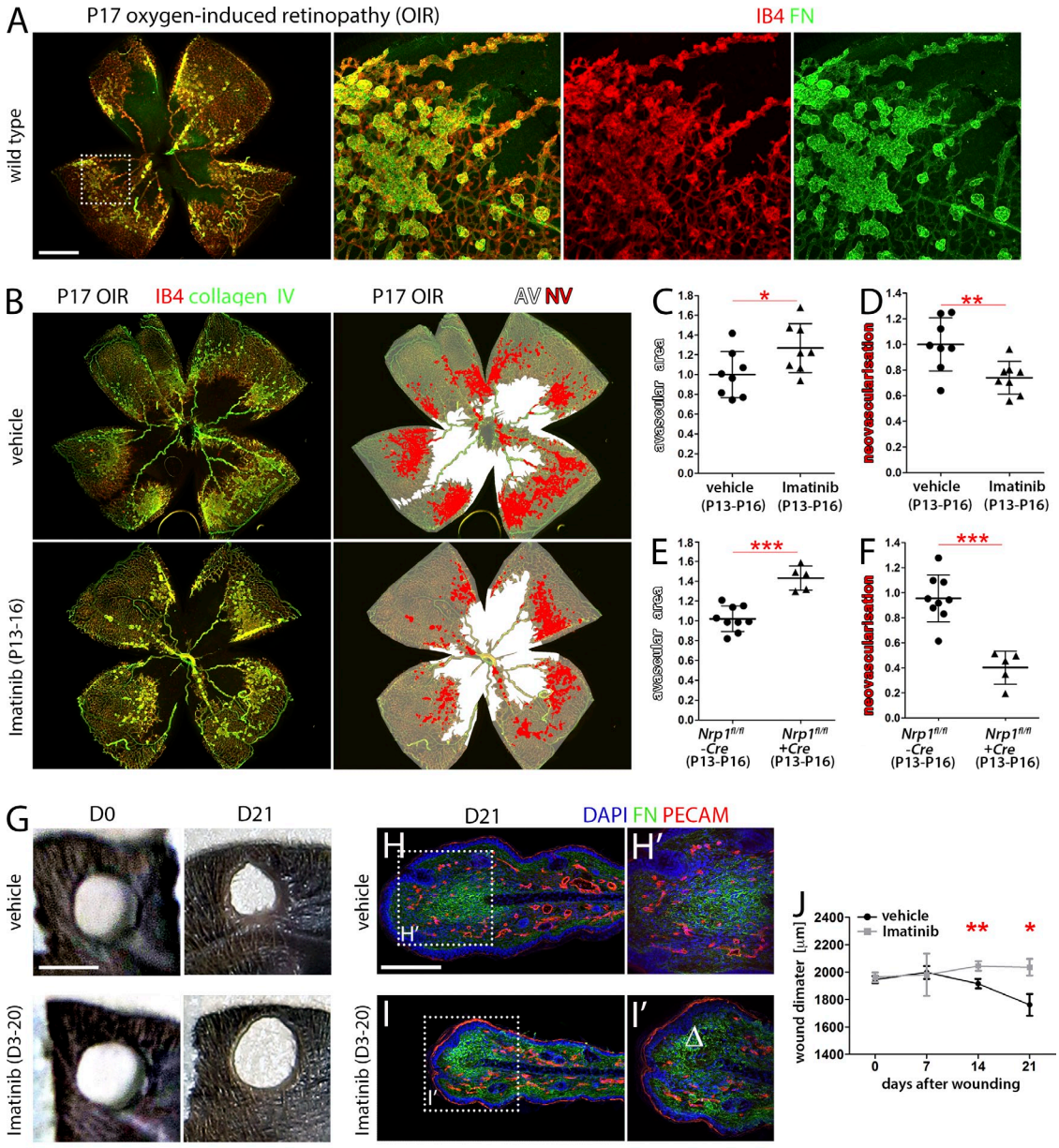

Figure 8. Imatinib and endothelial NRP1 targeting inhibit pathological angiogenesis in mouse models of retinopathy and ear wound healing. (A) Immunostaining of a P17 wild-type mouse retina for FN together with IB4 after sequential exposure to 7 d of normoxia, 5 d of hyperoxia, and 5 d of normoxia. The area indicated with a square is shown in higher magnification adjacent to the first panel as double label and single channels. Bar, 1 mm. (B) Immunostaining for collagen IV together with IB4 of P17 retinas from mice treated with vehicle (control) or Imatinib by daily injections after return from hyperoxia to normoxia (P13–16). Pseudocoloring highlights AV (white) and neovascularization (NV, red). Bar, 1 mm. (C–F) Quantitation of AV and NV area in Imatinib-treated relative to vehicle-injected littermates (C and D; fold change; $n = 8$ retinas each) and in tamoxifen-injected *Nrp1*$^{fl/fl}$ mice lacking or expressing *Pdgfb-iCre-ERT2-Egfp* (E and F; fold change; $n \geq 5$ retinas each). Asterisks indicate statistical significance: *, $P < 0.05$; **, $P < 0.01$; ***, $P < 0.001$, Student's *t* test. Error bars show SD. (G–J) To examine angiogenesis-dependent wound healing in the ear of vehicle- and Imatinib-treated mice between the day of injury (day 0, D0) and day 21, the punch wound was imaged on days 0 and 21 (G; bar, 2 mm) and immunostained for FN together with PECAM and DAPI in 40-µm ear sections on day 21 (H and I; bar, 200 µm). Higher magnifications of the areas indicated with dotted squares in H and I are shown in H′ and I′. Note the reduced number of blood vessels at the wound margin after Imatinib treatment (Δ). (J) Quantitation of wound diameter in vehicle and Imatinib-treated mice on days 0, 7, 14, and 21 after wounding (vehicle, $n = 3$ mice; Imatinib, $n = 4$ mice; *, $P < 0.05$; **, $P < 0.01$, Student's *t* test for vehicle vs. Imatinib-treated mice at days 14 and 21). Error bars show SEM.

which the healing of ear punch injuries depends on neoangiogenesis (Cho et al., 2006) and the wound margin is rich in FN (Fig. 8 H). Daily Imatinib treatment of adult mice from day 3 until day 20 after ear punch inhibited wound closure, with a significantly larger wound diameter at both 14 and 21 d compared with vehicle-treated controls (Fig. 8, H and J).

Although FN deposition at the wound was not obviously affected by Imatinib treatment, blood vessel density in the wound margin was reduced (Fig. 8, H–I′). Imatinib therefore targets pathological vessel growth in both the eye and skin.

DISCUSSION

In vertebrates, organ formation and homeostasis require the delivery of oxygen and nutrients through blood vessel networks, which form in response to signals provided by the vascular endothelial growth factor VEGF (Ruhrberg, 2003). VEGF-driven vascular morphogenesis entails the processes of vasculogenesis, angiogenesis, and arteriogenesis, which all rely on signal transduction by the VEGF receptor tyrosine kinase VEGFR2 (Koch et al., 2011). However, it is poorly understood how VEGF signaling is integrated with other signaling pathways to ensure that these complementary processes take place in appropriate contexts (Carmeliet and Jain, 2011). We show here that the VEGF receptor NRP1 has an unexpected role in a non-VEGF–driven angiogenesis pathway that is activated by ECM signals and involves the tyrosine kinase ABL1. The discovery of this pathway has important implications for our understanding of both physiological and pathological vessel growth.

The coactivation of VEGF-induced and ECM-stimulated signaling pathways benefits ordered blood vessel growth in complex tissues. Thus, it was previously shown that endothelial tip cells extend filopodia to sense VEGF gradients and to align themselves along matrix templates for directional migration (Ruhrberg et al., 2002; Gerhardt et al., 2003; Uemura et al., 2006; Stenzel et al., 2011). Moreover, signaling responses induced by ECM-bound VEGF165 involve integrin activation and differ mechanistically from those induced by soluble VEGF165 (Chen et al., 2010). However, the functional significance of NRP1's ability to associate with integrins independently of VEGFR2 (Soker et al., 2002; Fukasawa et al., 2007; Robinson et al., 2009; Valdembri et al., 2009) was not previously understood. We demonstrate here that NRP1 promotes integrin ligand-induced EC motility in a VEGFR2-independent mechanism that involves ABL1-dependent PXN phosphorylation, focal adhesion formation, and actin remodeling. We further show that this pathway is essential for normal vessel sprouting and vascular plexus formation in vivo. NRP1 therefore has a dual role in ECs by contributing to both VEGF-dependent VEGFR2 activation and ECM-stimulated but VEGF/VEGFR2-independent signaling via ABL1.

The novel proangiogenic NRP1 function we have identified differs fundamentally from prior models, which proposed that endothelial NRP1 acts exclusively as a VEGF coreceptor to enhance VEGFR2 signaling. Collectively with recent findings that NRP1 associates with VEGFR2 to stimulate VEGF-induced arteriogenesis (Lanahan et al., 2013), endothelial NRP1 appears to activate specific tyrosine kinase pathways in a context-dependent fashion to regulate vascular morphogenesis. The existence of an ABL1-dependent but VEGFR2-independent role for NRP1 in angiogenesis may also explain why blood vessel growth is affected more severely by loss of NRP1 than loss of NRP1-binding VEGF isoforms (Ruhrberg et al., 2002; Gerhardt et al., 2004; Raimondi and Ruhrberg, 2013), why the loss of VEGF binding to NRP1 causes milder embryonic vascular defects than loss of NRP1 (Fantin et al., 2014), and why anti-NRP1 and anti-VEGF treatments synergize to block angiogenesis-dependent tumor growth (Pan et al., 2007a). Importantly, our finding that NRP1 mediates ABL1 signaling to regulate actin cytoskeleton and cell migration in response to extracellular signals has far reaching implications beyond understanding angiogenesis, as NRP1 is important for the behavior of diverse cell types, including immune cells, neural crest cells, neurons, and tumor cells.

VEGFR2-independent functions of NRP1 in ECs in vitro have previously been ascribed to NRP1 cytoplasmic domain signaling. For example, the extracellular part of the EGF receptor, when linked to the NRP1 transmembrane and cytoplasmic domains, enables EGF-stimulated EC migration (Wang et al., 2006). The cytoplasmic NRP1 domain also promotes FN fibrillogenesis in arterial ECs by regulating endosomal trafficking of activated α5β1 integrin (Valdembri et al., 2009) and is involved in ABL1-mediated FN fibrillogenesis in myofibroblasts (Yaqoob et al., 2012). However, NRP1 cytoplasmic domain–mediated signal transduction pathways or integrin endocytosis are unlikely to play major roles in angiogenesis because genetic mouse studies showed that this NRP1 domain is dispensable for physiological and pathological angiogenesis (Fantin et al., 2011; Lanahan et al., 2013). Instead, NRP1 contributes to angiogenesis solely via its membrane-tethered extracellular domain (Fantin et al., 2011). Our finding that NRP1 promotes matrix signaling to enhance angiogenesis therefore agrees with prior observations that the extracellular rather than intracellular NRP1 interacts with α5β1 integrin (Fukasawa et al., 2007; Valdembri et al., 2009). Because the NRP1 extracellular domain complexes with integrins, but the NRP1 cytoplasmic tail is not required for angiogenesis, NRP1 most likely associates with ABL1 indirectly, possibly via integrins, as they are known to recruit ABL1 (Cui et al., 2009; Baruzzi et al., 2010).

The NRP1 dependency of FN-stimulated EC motility and migration was reflected in the defective activation of several previously identified integrin targets in NRP1 knockdown cells, including PLCγ1, ABL1, and PXN. However, targeting the FN-stimulated NRP1–ABL1 pathway impaired retinal angiogenesis more severely than deleting astrocytic FN or single integrins (Stenzel et al., 2011). The greater dependency of angiogenesis on NRP1 than on individual ECM components or different integrins may be explained by the partial redundancy of proangiogenic matrix components for at least some signaling responses (Stenzel et al., 2011) and the presence of multiple endothelial FN receptors, including α5β1 and αvβ3 (Dejana et al., 1990). Moreover, NRP1 can itself act as an adhesion receptor (Shimizu et al., 2000).

Our study identified endothelial NRP1 as a bimodal regulator of vascular morphogenesis that regulates ABL1-mediated signal transduction and actin remodeling during angiogenesis, even though it promotes VEGFR2 trafficking and signaling

during arteriogenesis. In addition to regulating physiological vessel growth, the NRP1–ABL1 pathway promotes vascular pathology that can be inhibited by treatment with Imatinib, a small molecule inhibitor of ABL1, or through the genetic ablation of NRP1 in ECs; thus, both approaches significantly and similarly reduced vessel growth in a mouse model of human retinopathy. Targeting NRP1-mediated ABL1 signaling might therefore provide a novel therapeutic opportunity to enhance the efficacy of current anti-angiogenic therapies that focus on manipulating VEGF signaling through VEGFR2, for example to inhibit tumor angiogenesis or neovascular eye disease. In particular, the FDA-approved drug Imatinib might provide a complementary treatment to improve the responsiveness of patients to anti-angiogenic therapies, for example in metastatic colon cancer, PDR, or AMD. Additionally, Imatinib treatment may be beneficial for patients with cancers that are fuelled by vasculature that is resistant to anti-VEGF therapy. As shown in this preclinical study, Imatinib might be delivered systemically to treat vascular eye pathology to circumvent complications of intravitreal administration of anti-VEGF therapies, such as increased intraocular pressure or endophthalmitis. In conclusion, the unexpected finding that NRP1 promotes angiogenesis in a VEGFR2-independent fashion via ABL1 supports a model in which NRP1-mediated ECM signaling proceeds independently of, but synergistically with, VEGFR2-mediated growth factor signaling to drive angiogenic tissue invasion in development and disease (Fig. 7 H).

MATERIALS AND METHODS

Cell culture, transfection, and adenovirus infection. HDMECs (Promocell) were cultured in MV2 media with supplements (Promocell). HUVECs (Promocell) were cultured in EBM2 media (Lonza) containing 10% FBS (Life Technologies), 300 µg/ml EC growth supplement (ECGS; Sigma-Aldrich), and 1 µg/ml hydrocortisone (Sigma-Aldrich). Cells were transfected with lipofectamine RNAIMAX using SMARTpool siRNA targeting NRP1,VEGFR2, or ABL1 (Dharmacon), or Silencer negative control siRNA (Applied Biosystems). For overexpression studies, HDMECs were transfected with Lipofectamine according to the manufacturer's protocol. In some experiments, cells were incubated with 10 µM Imatinib (Cambridge Bioscience), a concentration known to effectively target ABL1 kinase (Chislock et al., 2013). In some experiments, cells were stimulated with 50 ng/ml VEGF165 for the indicated times. Primary MLECs were isolated from mice between 1 and 2 mo of age by magnetic-activated cell sorting (MACS) with PECAM antibodies (BD). MLECs were cultured on 10 µg/ml FN in DMEM-GlutaMAX supplemented with 20% FBS, nonessential amino acids (Life Technologies), and ECGS. MLECs from *Nrp1*$^{fl/fl}$ conditional null mice were infected with adenovirus-expressing CRE recombinase or with control virus–expressing GFP, incubated for 24 h in culture media, washed in PBS, and cultured in fresh media for 48 h before migration and immunoblotting experiments.

Adhesion assay. HUVECs or HDMECs transfected with targeting or control siRNA were detached with trypsin, resuspended in MV2 medium containing 0.5% BSA, and incubated at 37°C for 1 h on a rotating wheel. 10,000 cells/well were seeded on 96-well tissue culture plates (Nunc;Thermo Fisher Scientific) coated overnight with 10 µg/ml FN in PBS or, as an internal control, PBS containing 1% BSA, for the indicated times in triplicate, washed in PBS, fixed in 4% formaldehyde in PBS, and stained with 0.1% crystal violet for 30 min. After washing three times with PBS for 15 min, dye was extracted with 10% SDS in PBS for 15 min on an orbital shaker to determine absorbance at 570 nm.

Cell migration assay. HDMECs were transfected with siRNA and MLECs treated with adenovirus before overnight serum starvation and then plated onto FN-coated transwell inserts (8.0 µm pores, 10 mm diameter; Nunc) that had been preincubated with MV2 containing 0.5% BSA (HDMECs) or DMEM containing 0.5% BSA (MLECs). After 4 h, cells on the upper face of the insert were removed with a cotton bud, while transmigrated cells on the underside were fixed with 4% formaldehyde in PBS for 10 min and stained with 0.1% crystal violet solution for 10 min. Images were acquired with a phase-contrast light microscope using a c-plan 10×/0.22 objective (Leica). Transmigrated cells in duplicate inserts were counted in a minimum of five images per insert in three independent experiments.

Random motility. HDMECs were transfected with siRNA, serum-starved overnight 56 h after transfection, and then detached and seeded in duplicates into 6-well plates that had been coated overnight with 10 µg/ml FN. Cells were then imaged in an environmental chamber maintaining a 5% CO_2 atmosphere at 37°C with a 10× phase contrast objective at 2-min intervals for 200 min using an inverted phase contrast microscope (Axiovert-200M; Carl Zeiss). The motility of 25 cells per each condition from two experiments was analyzed using the ImageJ MTrackJ extension module (National Institutes of Health).

Phosphokinase antibody array. HDMECs were transfected with siRNA. 56 h after transfection, cells were serum-starved overnight and then stimulated with 50 ng/ml VEGF165 for 10 min or detached using 0.5× trypsin/EDTA (PAA), resuspended in MV2 serum-free media, and plated for 30 min on tissue culture plates coated with 10 µg/ml FN. ECs were lysed as described in Immunoblotting and immunoprecipitation and phosphokinase antibody array was performed according to the manufacturer's instructions (R&D Systems).

Gene expression. mRNA was extracted using the RNeasy system (QIAGEN). cDNA was prepared using Superscript II reverse transcription (Invitrogen) and amplified with (SYBR Green; Applied Biosystems) and the following oligonucleotide primers: *NRP1*, 5′-GAAAAATCGAATGCTGAT-3′ and 5′-AATCCGGGGGACTTTATCAC-3′; *ABL1*, 5′-GAGGGCGTGTGGAAGAAATA-3′ and 5′-GGTAGCAATTTCCCAAAGCA-3′; *VEGFR2*, 5′-AGATGGTGTAACCCGGAGTG-3′ and 5′-ACATGTCAGCGTTTGAGTGG-3′; and *GUS*, 5′-AAACGATTGCAGGGTTTCAC-3′ and 5′-CTCTCGTCGGTGACTGTTCA-3′. Gene expression was analyzed with the quantitative 7500 Real-Time PCR System (Applied Biosystems). Data analysis was performed using the SDS software (version 2.3; Applied Biosystems).

Immunoblotting and immunoprecipitation. Cells were lysed with lysis buffer (50 mM Tris-HCl, pH 7.4, 5 mM EDTA, 0.1% NP-40, and 250 mM NaCl) in the presence of protease inhibitor cocktail 2 and phosphatase inhibitor cocktail (Sigma-Aldrich). Lungs from P7 mice were lysed in GL35 (Cytoskeleton, Inc). 25 µg of protein was resuspended in Laemmli sample buffer, denatured for 5 min, separated by SDS-PAGE, and transferred to nitrocellulose membrane (Whatman).

Protein extracts were analyzed by SDS-PAGE and transferred to nitrocellulose membrane (Whatman) for immunoblotting with the following primary antibodies: rabbit anti-GAPDH (Abcam), goat anti-NRP1 C-19 (Santa Cruz Biotechnology, Inc.) or AF566 (R&D Systems); mouse anti-ABL1 (BD); rabbit anti-pCRKL (Y207), rabbit anti-pKDR (Y1175) or KDR, rabbit anti-pPXN (Y118), rabbit anti-pAKT (S473) or AKT, or rabbit anti-pERK1/2 or ERK1/2 (Cell Signaling Technology).

Immunoprecipitation. Serum-starved ECs were detached with 0.5× trypsin/EDTA and lysed or seeded into FN-coated plastic dishes for the indicated times before lysis. In some experiments, ECs were treated with 10 µM Imatinib (Glivec; Cambridge Bioscience) for 30 min before and during FN stimulation. ECs were lysed in 50 mM Tris, pH 8.0, 50 mM KCl, 1% (vol/vol) NP-40 in the presence of protease inhibitor cocktail 2 and phosphatase inhibitor cocktail. 1 mg of protein was incubated with 3 µg goat anti-NRP1 (Fantin et al., 2010), rabbit anti-ABL1 (Roig et al., 2000), or control goat or rabbit IgG (Santa Cruz Biotechnology) and then with 30 µl

magnetic protein G Dynabeads (Life Technologies) at 4°C. Beads were collected with a Dynabead magnet, washed three times with lysis buffer on a rotating wheel at 4°C for 5 min, and resuspended in 50 µl Laemmli sample buffer for SDS-PAGE and immunoblotting.

Immunofluorescence. HDMECs were transfected with siRNA. 56 h after transfection, cells were serum-starved overnight, detached using 0.5× trypsin/EDTA, resuspended in MV2, and seeded on FN-coated coverslips for various time points. ECs were fixed in 4% formaldehyde in PBS for 30 min, permeabilized in PBS containing 0.25% Triton X-100 for 2 min, and then stained with rabbit anti-pPXN or mouse anti-NRP1 (R&D Systems), followed by Alexa Fluor 594–conjugated goat anti–rabbit or anti–mouse antibodies (Life Technologies) and FITC-conjugated phalloidin (Sigma-Aldrich). Images were acquired with a Plan Apochromat 63× 1.4 NA oil objective on a LSM700 confocal microscope (Carl Zeiss). P6 mouse retinas or 20-µm cryosections through ear wounds were immunolabeled as described (Fantin et al., 2011) using rabbit anti-pPXN or rabbit anti-FN (Abcam) together with biotinylated isolectin B4 (IB4; Sigma-Aldrich) or rat anti-PECAM (BD), followed by Alexa Fluor 594– or 488–conjugated goat anti–rabbit or anti–rat antibodies and Alexa Fluor 647–conjugated streptavidin (Life Technologies). Confocal z-stacks were acquired with a laser scanning confocal microscope (LSM710; Carl Zeiss). FN mean pixel intensity in nonsaturated maximal intensity projections was determined with ImageJ for an area of 0.06 mm^2 ahead of the vascular front and plotted as fold change compared with control. Endothelial pPXN or FN staining were isolated by virtually masking out nonendothelial staining after IB4 surface rendering with IMARIS (Bitplan AG) and expressed as relative to IB4 mean pixel intensity.

Animals. All animal procedures were performed in accordance with institutional and UK Home Office guidelines. We used C57BL/6 wild-type mice (Charles River), littermate wild-type and heterozygous *Nrp1*-null mutants (Kitsukawa et al., 1997), and mice carrying two floxed conditional null *Nrp1* alleles (*Nrp1*$^{fl/fl}$) combined with *Pdgfb-iCre-ERT2-Egfp* with codon-improved *Cre* on a C57BL/6 background (Fantin et al., 2013). For tamoxifen induction of CRE-mediated recombination, 0.2 mg of tamoxifen (Sigma-Aldrich) dissolved in peanut oil to 2 mg/ml was administered via intraperitoneal injection into pups at the indicated times. In some experiments, mice were injected intraperitoneally with 100 mg/kg/d Imatinib in 0.9% saline solution for the indicated times. We induced OIR as previously described (Connor et al., 2009). In brief, nursing dams and their pups were maintained at 75 ± 3% O_2 in an oxygen supply chamber from P7 to P12; dams were rested in room air for 1 h each day. Dams and pups were returned to room air on P12 and the pups culled on P17 to isolate retinas for immunolabeling; the size of the avascular and neovascular areas was determined with Photoshop (CS4; Adobe) in images acquired with a stereo fluorescent microscope (SZX16; Olympus) equipped with a digital camera (Hamamatsu Photonics). Ear wound healing was assessed in adult mice with a 2-mm hole in the ear center, which was made with a metal ear punch to identify mice during standard mouse husbandry.

Statistical analyses. Statistical analyses were performed with Prism (GraphPad Software) or Excel (Microsoft). Data obtained from cell lines were analyzed with a two-tailed, paired Student's *t* test, whereas data from retina samples were analyzed using a two-tailed, unpaired Student's *t* test or ANOVA.

Online supplemental material. Video 1 shows images of HDMECs transfected with control siRNAs that were acquired every 2 min for 200 min. Video 2 shows images of HDMECs transfected with NRP1 targeting siRNAs that were acquired every 2 min for 200 min. Online supplemental material is available at http://www.jem.org/cgi/content/full/jem.20132330/DC1.

We are grateful to the staff of the Biological Resources Unit at the UCL Institute of Ophthalmology for help with mouse husbandry and thank the Imaging Facility at the UCL Institute of Ophthalmology for maintenance of the confocal microscopes. We also thank Michael Simons and John Greenwood for critical reading of the manuscript.

This study was supported by a research fellowship from the British Heart Foundation to C. Raimondi (FS/13/35/30148), a research grant from the British Heart Foundation to C. Ruhrberg (PG/10/86/28622), and a New Investigator Award from the Wellcome Trust to C. Ruhrberg (095623/Z/11/Z).

The authors declare no competing financial interests.

Author contributions: C. Raimondi, A. Fantin, and C. Ruhrberg designed the research, performed the research, analyzed the data, and wrote the manuscript. A. Lampropoulou performed research and analyzed the data. L. Denti performed research. A. Chikh designed and performed research.

Submitted: 7 November 2013
Accepted: 14 April 2014

REFERENCES

Anselmi, F., M. Orlandini, M. Rocchigiani, C. De Clemente, A. Salameh, C. Lentucci, S. Oliviero, and F. Galvagni. 2012. c-ABL modulates MAP kinases activation downstream of VEGFR-2 signaling by direct phosphorylation of the adaptor proteins GRB2 and NCK1. *Angiogenesis*. 15:187–197. http://dx.doi.org/10.1007/s10456-012-9252-6

Ballmer-Hofer, K., A.E. Andersson, L.E. Ratcliffe, and P. Berger. 2011. Neuropilin-1 promotes VEGFR-2 trafficking through Rab11 vesicles thereby specifying signal output. *Blood*. 118:816–826. http://dx.doi.org/10.1182/blood-2011-01-328773

Baruzzi, A., I. Iacobucci, S. Soverini, C.A. Lowell, G. Martinelli, and G. Berton. 2010. c-Abl and Src-family kinases cross-talk in regulation of myeloid cell migration. *FEBS Lett*. 584:15–21. http://dx.doi.org/10.1016/j.febslet.2009.11.009

Birukova, A.A., I. Cokic, N. Moldobaeva, and K.G. Birukov. 2009. Paxillin is involved in the differential regulation of endothelial barrier by HGF and VEGF. *Am. J. Respir. Cell Mol. Biol.* 40:99–107. http://dx.doi.org/10.1165/rcmb.2008-0099OC

Buchdunger, E., T. O'Reilly, and J. Wood. 2002. Pharmacology of imatinib (STI571). *Eur. J. Cancer*. 38(Suppl 5):S28–S36. http://dx.doi.org/10.1016/S0959-8049(02)80600-1

Campochiaro, P.A. 2013. Ocular neovascularization. *J. Mol. Med*. 91:311–321. http://dx.doi.org/10.1007/s00109-013-0993-5

Carmeliet, P., and R.K. Jain. 2011. Molecular mechanisms and clinical applications of angiogenesis. *Nature*. 473:298–307. http://dx.doi.org/10.1038/nature10144

Casanovas, O., D.J. Hicklin, G. Bergers, and D. Hanahan. 2005. Drug resistance by evasion of antiangiogenic targeting of VEGF signaling in late-stage pancreatic islet tumors. *Cancer Cell*. 8:299–309. http://dx.doi.org/10.1016/j.ccr.2005.09.005

Chen, H.C., P.A. Appeddu, H. Isoda, and J.L. Guan. 1996. Phosphorylation of tyrosine 397 in focal adhesion kinase is required for binding phosphatidylinositol 3-kinase. *J. Biol Chem*. 271:26329–26334. http://dx.doi.org/10.1074/jbc.271.42.26329

Chen, T.T., A. Luque, S. Lee, S.M. Anderson, T. Segura, and M.L. Iruela-Arispe. 2010. Anchorage of VEGF to the extracellular matrix conveys differential signaling responses to endothelial cells. *J. Cell Biol*. 188:595–609. http://dx.doi.org/10.1083/jcb.200906044

Chislock, E.M., C. Ring, and A.M. Pendergast. 2013. Abl kinases are required for vascular function, Tie2 expression, and angiopoietin-1–mediated survival. *Proc. Natl. Acad. Sci. USA*. 110:12432–12437. http://dx.doi.org/10.1073/pnas.1304188110

Cho, C.H., H.K. Sung, K.T. Kim, H.G. Cheon, G.T. Oh, H.J. Hong, O.J. Yoo, and G.Y. Koh. 2006. COMP-angiopoietin-1 promotes wound healing through enhanced angiogenesis, lymphangiogenesis, and blood flow in a diabetic mouse model. *Proc. Natl. Acad. Sci. USA*. 103:4946–4951. http://dx.doi.org/10.1073/pnas.0506352103

Choi, J.H., Y.R. Yang, S.K. Lee, I.S. Kim, S.H. Ha, E.K. Kim, Y.S. Bae, S.H. Ryu, and P.G. Suh. 2007. Phospholipase C-γ1 potentiates integrin-dependent cell spreading and migration through Pyk2/paxillin activation. *Cell. Signal*. 19:1784–1796. http://dx.doi.org/10.1016/j.cellsig.2007.04.002

Clark, R.A., R.J. Mason, J.M. Folkvord, and J.A. McDonald. 1986. Fibronectin mediates adherence of rat alveolar type II epithelial cells via the fibroblastic cell-attachment domain. *J. Clin. Invest*. 77:1831–1840. http://dx.doi.org/10.1172/JCI112509

Colicelli, J. 2010. ABL tyrosine kinases: evolution of function, regulation, and specificity. *Sci. Signal.* 3:re6. http://dx.doi.org/10.1126/scisignal.3139re6

Connor, K.M., N.M. Krah, R.J. Dennison, C.M. Aderman, J. Chen, K.I. Guerin, P. Sapieha, A. Stahl, K.L. Willett, and L.E. Smith. 2009. Quantification of oxygen-induced retinopathy in the mouse: a model of vessel loss, vessel regrowth and pathological angiogenesis. *Nat. Protoc.* 4:1565–1573. http://dx.doi.org/10.1038/nprot.2009.187

Cui, L., C. Chen, T. Xu, J. Zhang, X. Shang, J. Luo, L. Chen, X. Ba, and X. Zeng. 2009. c-Abl kinase is required for β_2 integrin-mediated neutrophil adhesion. *J. Immunol.* 182:3233–3242. http://dx.doi.org/10.4049/jimmunol.0802621

Cujec, T.P., P.F. Medeiros, P. Hammond, C. Rise, and B.L. Kreider. 2002. Selection of v-abl tyrosine kinase substrate sequences from randomized peptide and cellular proteomic libraries using mRNA display. *Chem. Biol.* 9:253–264. http://dx.doi.org/10.1016/S1074-5521(02)00098-4

Dejana, E., M.G. Lampugnani, M. Giorgi, M. Gaboli, and P.C. Marchisio. 1990. Fibrinogen induces endothelial cell adhesion and spreading via the release of endogenous matrix proteins and the recruitment of more than one integrin receptor. *Blood.* 75:1509–1517.

Druker, B.J., S. Tamura, E. Buchdunger, S. Ohno, G.M. Segal, S. Fanning, J. Zimmermann, and N.B. Lydon. 1996. Effects of a selective inhibitor of the Abl tyrosine kinase on the growth of Bcr-Abl positive cells. *Nat. Med.* 2:561–566. http://dx.doi.org/10.1038/nm0596-561

Fantin, A., J.M. Vieira, G. Gestri, L. Denti, Q. Schwarz, S. Prykhozhij, F. Peri, S.W. Wilson, and C. Ruhrberg. 2010. Tissue macrophages act as cellular chaperones for vascular anastomosis downstream of VEGF-mediated endothelial tip cell induction. *Blood.* 116:829–840. http://dx.doi.org/10.1182/blood-2009-12-257832

Fantin, A., Q. Schwarz, K. Davidson, E.M. Normando, L. Denti, and C. Ruhrberg. 2011. The cytoplasmic domain of neuropilin 1 is dispensable for angiogenesis, but promotes the spatial separation of retinal arteries and veins. *Development.* 138:4185–4191. http://dx.doi.org/10.1242/dev.070037

Fantin, A., J.M. Vieira, A. Plein, L. Denti, M. Fruttiger, J.W. Pollard, and C. Ruhrberg. 2013. NRP1 acts cell autonomously in endothelium to promote tip cell function during sprouting angiogenesis. *Blood.* 121:2352–2362. http://dx.doi.org/10.1182/blood-2012-05-424713

Fantin, A., B. Herzog, M. Mahmoud, M. Yamaji, A. Plein, L. Denti, C. Ruhrberg, and I. Zachary. 2014. Neuropilin 1 (NRP1) hypomorphism combined with defective VEGF-A binding reveals novel roles for NRP1 in developmental and pathological angiogenesis. *Development.* 141:556–562. http://dx.doi.org/10.1242/dev.103028

Foxton, R.H., A. Finkelstein, S. Vijay, A. Dahlmann-Noor, P.T. Khaw, J.E. Morgan, D.T. Shima, and Y.S. Ng. 2013. VEGF-A is necessary and sufficient for retinal neuroprotection in models of experimental glaucoma. *Am. J. Pathol.* 182:1379–1390. http://dx.doi.org/10.1016/j.ajpath.2012.12.032

Fukasawa, M., A. Matsushita, and M. Korc. 2007. Neuropilin-1 interacts with integrin beta1 and modulates pancreatic cancer cell growth, survival and invasion. *Cancer Biol. Ther.* 6:1184–1191. http://dx.doi.org/10.4161/cbt.6.8.4363

Gerhardt, H., M. Golding, M. Fruttiger, C. Ruhrberg, A. Lundkvist, A. Abramsson, M. Jeltsch, C. Mitchell, K. Alitalo, D. Shima, and C. Betsholtz. 2003. VEGF guides angiogenic sprouting utilizing endothelial tip cell filopodia. *J. Cell Biol.* 161:1163–1177. http://dx.doi.org/10.1083/jcb.200302047

Gerhardt, H., C. Ruhrberg, A. Abramsson, H. Fujisawa, D. Shima, and C. Betsholtz. 2004. Neuropilin-1 is required for endothelial tip cell guidance in the developing central nervous system. *Dev. Dyn.* 231:503–509. http://dx.doi.org/10.1002/dvdy.20148

Herzog, B., C. Pellet-Many, G. Britton, B. Hartzoulakis, and I.C. Zachary. 2011. VEGF binding to NRP1 is essential for VEGF stimulation of endothelial cell migration, complex formation between NRP1 and VEGFR2, and signaling via FAK Tyr407 phosphorylation. *Mol. Biol. Cell.* 22:2766–2776. http://dx.doi.org/10.1091/mbc.E09-12-1061

Kawamura, H., X. Li, K. Goishi, L.A. van Meeteren, L. Jakobsson, S. Cébe-Suarez, A. Shimizu, D. Edholm, K. Ballmer-Hofer, L. Kjellén, et al. 2008. Neuropilin-1 in regulation of VEGF-induced activation of p38MAPK and endothelial cell organization. *Blood.* 112:3638–3649. http://dx.doi.org/10.1182/blood-2007-12-125856

Kawasaki, T., T. Kitsukawa, Y. Bekku, Y. Matsuda, M. Sanbo, T. Yagi, and H. Fujisawa. 1999. A requirement for neuropilin-1 in embryonic vessel formation. *Development.* 126:4895–4902.

Kim, L.A., and P.A. D'Amore. 2012. A brief history of anti-VEGF for the treatment of ocular angiogenesis. *Am. J. Pathol.* 181:376–379. http://dx.doi.org/10.1016/j.ajpath.2012.06.006

Kitsukawa, T., M. Shimizu, M. Sanbo, T. Hirata, M. Taniguchi, Y. Bekku, T. Yagi, and H. Fujisawa. 1997. Neuropilin-semaphorin III/D-mediated chemorepulsive signals play a crucial role in peripheral nerve projection in mice. *Neuron.* 19:995–1005. http://dx.doi.org/10.1016/S0896-6273(00)80392-X

Koch, S., S. Tugues, X. Li, L. Gualandi, and L. Claesson-Welsh. 2011. Signal transduction by vascular endothelial growth factor receptors. *Biochem. J.* 437:169–183. http://dx.doi.org/10.1042/BJ20110301

Lanahan, A.A., K. Hermans, F. Claes, J.S. Kerley-Hamilton, Z.W. Zhuang, F.J. Giordano, P. Carmeliet, and M. Simons. 2010. VEGF receptor 2 endocytic trafficking regulates arterial morphogenesis. *Dev. Cell.* 18:713–724. http://dx.doi.org/10.1016/j.devcel.2010.02.016

Lanahan, A., X. Zhang, A. Fantin, Z. Zhuang, F. Rivera-Molina, K. Speichinger, C. Prahst, J. Zhang, Y. Wang, G. Davis, et al. 2013. The neuropilin 1 cytoplasmic domain is required for VEGF-A-dependent arteriogenesis. *Dev. Cell.* 25:156–168. http://dx.doi.org/10.1016/j.devcel.2013.03.019

Lewis, J.M., and M.A. Schwartz. 1998. Integrins regulate the association and phosphorylation of paxillin by c-Abl. *J. Biol. Chem.* 273:14225–14230. http://dx.doi.org/10.1074/jbc.273.23.14225

Lewis, J.M., R. Baskaran, S. Taagepera, M.A. Schwartz, and J.Y. Wang. 1996. Integrin regulation of c-Abl tyrosine kinase activity and cytoplasmic-nuclear transport. *Proc. Natl. Acad. Sci. USA.* 93:15174–15179. http://dx.doi.org/10.1073/pnas.93.26.15174

Mamluk, R., Z. Gechtman, M.E. Kutcher, N. Gasiunas, J. Gallagher, and M. Klagsbrun. 2002. Neuropilin-1 binds vascular endothelial growth factor 165, placenta growth factor-2, and heparin via its b1b2 domain. *J. Biol. Chem.* 277:24818–24825. http://dx.doi.org/10.1074/jbc.M200730200

Murga, M., O. Fernandez-Capetillo, and G. Tosato. 2005. Neuropilin-1 regulates attachment in human endothelial cells independently of vascular endothelial growth factor receptor-2. *Blood.* 105:1992–1999. http://dx.doi.org/10.1182/blood-2004-07-2598

Nishijima, K., Y.S. Ng, L. Zhong, J. Bradley, W. Schubert, N. Jo, J. Akita, S.J. Samuelsson, G.S. Robinson, A.P. Adamis, and D.T. Shima. 2007. Vascular endothelial growth factor-A is a survival factor for retinal neurons and a critical neuroprotectant during the adaptive response to ischemic injury. *Am. J. Pathol.* 171:53–67. http://dx.doi.org/10.2353/ajpath.2007.061237

Pan, Q., Y. Chanthery, W.C. Liang, S. Stawicki, J. Mak, N. Rathore, R.K. Tong, J. Kowalski, S.F. Yee, G. Pacheco, et al. 2007a. Blocking neuropilin-1 function has an additive effect with anti-VEGF to inhibit tumor growth. *Cancer Cell.* 11:53–67. http://dx.doi.org/10.1016/j.ccr.2006.10.018

Pan, Q., Y. Chathery, Y. Wu, N. Rathore, R.K. Tong, F. Peale, A. Bagri, M. Tessier-Lavigne, A.W. Koch, and R.J. Watts. 2007b. Neuropilin-1 binds to VEGF121 and regulates endothelial cell migration and sprouting. *J. Biol. Chem.* 282:24049–24056. http://dx.doi.org/10.1074/jbc.M703554200

Parsons, J.T., K.H. Martin, J.K. Slack, J.M. Taylor, and S.A. Weed. 2000. Focal adhesion kinase: a regulator of focal adhesion dynamics and cell movement. *Oncogene.* 19:5606–5613. http://dx.doi.org/10.1038/sj.onc.1203877

Pasapera, A.M., I.C. Schneider, E. Rericha, D.D. Schlaepfer, and C.M. Waterman. 2010. Myosin II activity regulates vinculin recruitment to focal adhesions through FAK-mediated paxillin phosphorylation. *J. Cell Biol.* 188:877–890. http://dx.doi.org/10.1083/jcb.200906012

Phng, L.K., F. Stanchi, and H. Gerhardt. 2013. Filopodia are dispensable for endothelial tip cell guidance. *Development.* 140:4031–4040. http://dx.doi.org/10.1242/dev.097352

Raimondi, C., and C. Ruhrberg. 2013. Neuropilin signalling in vessels, neurons and tumours. *Semin. Cell Dev. Biol.* 24:172–178. http://dx.doi.org/10.1016/j.semcdb.2013.01.001

Ren, B., Y. Deng, A. Mukhopadhyay, A.A. Lanahan, Z.W. Zhuang, K.L. Moodie, M.J. Mulligan-Kehoe, T.V. Byzova, R.T. Peterson, and M. Simons. 2010. ERK1/2-Akt1 crosstalk regulates arteriogenesis in mice and zebrafish. *J. Clin. Invest.* 120:1217–1228. http://dx.doi.org/10.1172/JCI39837

Robinson, S.D., L.E. Reynolds, V. Kostourou, A.R. Reynolds, R.G. da Silva, B. Tavora, M. Baker, J.F. Marshall, and K.M. Hodivala-Dilke. 2009. Alphav β3 integrin limits the contribution of neuropilin-1 to vascular endothelial growth factor-induced angiogenesis. *J. Biol. Chem.* 284:33966–33981. http://dx.doi.org/10.1074/jbc.M109.030700

Roig, J., P.T. Tuazon, P.A. Zipfel, A.M. Pendergast, and J.A. Traugh. 2000. Functional interaction between c-Abl and the p21-activated protein kinase gamma-PAK. *Proc. Natl. Acad. Sci. USA.* 97:14346–14351. http://dx.doi.org/10.1073/pnas.97.26.14346

Rosenfeld, P.J., D.M. Brown, J.S. Heier, D.S. Boyer, P.K. Kaiser, C.Y. Chung, and R.Y. Kim; MARINA Study Group. 2006. Ranibizumab for neovascular age-related macular degeneration. *N. Engl. J. Med.* 355:1419–1431. http://dx.doi.org/10.1056/NEJMoa054481

Ruhrberg, C. 2003. Growing and shaping the vascular tree: multiple roles for VEGF. *Bioessays.* 25:1052–1060. http://dx.doi.org/10.1002/bies.10351

Ruhrberg, C., H. Gerhardt, M. Golding, R. Watson, S. Ioannidou, H. Fujisawa, C. Betsholtz, and D.T. Shima. 2002. Spatially restricted patterning cues provided by heparin-binding VEGF-A control blood vessel branching morphogenesis. *Genes Dev.* 16:2684–2698. http://dx.doi.org/10.1101/gad.242002

Saint-Geniez, M., A.S. Maharaj, T.E. Walshe, B.A. Tucker, E. Sekiyama, T. Kurihara, D.C. Darland, M.J. Young, and P.A. D'Amore. 2008. Endogenous VEGF is required for visual function: evidence for a survival role on müller cells and photoreceptors. *PLoS ONE.* 3:e3554. http://dx.doi.org/10.1371/journal.pone.0003554

Salikhova, A., L. Wang, A.A. Lanahan, M. Liu, M. Simons, W.P. Leenders, D. Mukhopadhyay, and A. Horowitz. 2008. Vascular endothelial growth factor and semaphorin induce neuropilin-1 endocytosis via separate pathways. *Circ. Res.* 103:e71–e79. http://dx.doi.org/10.1161/CIRCRESAHA.108.183327

Shimizu, M., Y. Murakami, F. Suto, and H. Fujisawa. 2000. Determination of cell adhesion sites of neuropilin-1. *J. Cell Biol.* 148:1283–1294. http://dx.doi.org/10.1083/jcb.148.6.1283

Shojaei, F., X. Wu, A.K. Malik, C. Zhong, M.E. Baldwin, S. Schanz, G. Fuh, H.P. Gerber, and N. Ferrara. 2007. Tumor refractoriness to anti-VEGF treatment is mediated by $CD11b^{+}Gr1^{+}$ myeloid cells. *Nat. Biotechnol.* 25:911–920. http://dx.doi.org/10.1038/nbt1323

Smith, L.E., E. Wesolowski, A. McLellan, S.K. Kostyk, R. D'Amato, R. Sullivan, and P.A. D'Amore. 1994. Oxygen-induced retinopathy in the mouse. *Invest. Ophthalmol. Vis. Sci.* 35:101–111.

Soker, S., H.Q. Miao, M. Nomi, S. Takashima, and M. Klagsbrun. 2002. VEGF165 mediates formation of complexes containing VEGFR-2 and neuropilin-1 that enhance VEGF165-receptor binding. *J. Cell. Biochem.* 85:357–368. http://dx.doi.org/10.1002/jcb.10140

Sottile, J., D.C. Hocking, and P.J. Swiatek. 1998. Fibronectin matrix assembly enhances adhesion-dependent cell growth. *J. Cell Sci.* 111:2933–2943.

Stenzel, D., A. Lundkvist, D. Sauvaget, M. Busse, M. Graupera, A. van der Flier, E.S. Wijelath, J. Murray, M. Sobel, M. Costell, et al. 2011. Integrin-dependent and -independent functions of astrocytic fibronectin in retinal angiogenesis. *Development.* 138:4451–4463. http://dx.doi.org/10.1242/dev.071381

Tvorogov, D., X.J. Wang, R. Zent, and G. Carpenter. 2005. Integrin-dependent PLC-γ1 phosphorylation mediates fibronectin-dependent adhesion. *J. Cell Sci.* 118:601–610. http://dx.doi.org/10.1242/jcs.01643

Uemura, A., S. Kusuhara, S.J. Wiegand, R.T. Yu, and S. Nishikawa. 2006. Tlx acts as a proangiogenic switch by regulating extracellular assembly of fibronectin matrices in retinal astrocytes. *J. Clin. Invest.* 116:369–377. http://dx.doi.org/10.1172/JCI25964

Valdembri, D., P.T. Caswell, K.I. Anderson, J.P. Schwarz, I. König, E. Astanina, F. Caccavari, J.C. Norman, M.J. Humphries, F. Bussolino, and G. Serini. 2009. Neuropilin-1/GIPC1 signaling regulates α5β1 integrin traffic and function in endothelial cells. *PLoS Biol.* 7:e25. http://dx.doi.org/10.1371/journal.pbio.1000025

Wang, L., D. Mukhopadhyay, and X. Xu. 2006. C terminus of RGS-GAIP-interacting protein conveys neuropilin-1-mediated signaling during angiogenesis. *FASEB J.* 20:1513–1515. http://dx.doi.org/10.1096/fj.05-5504fje

Welti, J., S. Loges, S. Dimmeler, and P. Carmeliet. 2013. Recent molecular discoveries in angiogenesis and antiangiogenic therapies in cancer. *J. Clin. Invest.* 123:3190–3200. http://dx.doi.org/10.1172/JCI70212

Yaqoob, U., S. Cao, U. Shergill, K. Jagavelu, Z. Geng, M. Yin, T.M. de Assuncao, Y. Cao, A. Szabolcs, S. Thorgeirsson, et al. 2012. Neuropilin-1 stimulates tumor growth by increasing fibronectin fibril assembly in the tumor microenvironment. *Cancer Res.* 72:4047–4059. http://dx.doi.org/10.1158/0008-5472.CAN-11-3907

Zaidel-Bar, R., R. Milo, Z. Kam, and B. Geiger. 2007. A paxillin tyrosine phosphorylation switch regulates the assembly and form of cell-matrix adhesions. *J. Cell Sci.* 120:137–148. http://dx.doi.org/10.1242/jcs.03314

Zhuang, G., X. Wu, Z. Jiang, I. Kasman, J. Yao, Y. Guan, J. Oeh, Z. Modrusan, C. Bais, D. Sampath, and N. Ferrara. 2012. Tumour-secreted miR-9 promotes endothelial cell migration and angiogenesis by activating the JAK-STAT pathway. *EMBO J.* 31:3513–3523. http://dx.doi.org/10.1038/emboj.2012.183